1 **BUB-1 and CENP-C recruit PLK-1 to Control Chromosome Alignment and Segregation**
2 **During Meiosis I in *C. elegans* Oocytes**
3
4 Samuel J.P. Taylor[1,a], Laura Bel Borja[1,a], Flavie Soubigou[1], Dhanya K. Cheerambathur[2], and
5 Federico Pelisch[1,*]
6
7 [1] Centre for Gene Regulation and Expression, Sir James Black Centre, School of Life
8 Sciences, University of Dundee. Dundee, DD1 5EH, United Kingdom
9 [2] Wellcome Centre for Cell Biology & Institute of Cell Biology, School of Biological Sciences, The
10 University of Edinburgh, Edinburgh, EH9 3BF, UK
11
12 [a] These authors contributed equally
13
14 * Corresponding author: Federico Pelisch (f.pelisch@dundee.ac.uk)

ABSTRACT

Phosphorylation is a key post-translational modification that is utilised in many biological processes for the rapid and reversible regulation of protein localisation and activity. Polo-like kinase 1 (PLK-1) is essential for both mitotic and meiotic cell divisions, with key functions being conserved in eukaryotes. The roles and regulation of PLK-1 during mitosis have been well characterised. However, the discrete roles and regulation of PLK-1 during meiosis have remained obscure. Here, we used *Caenorhabditis elegans (C. elegans)* oocytes to show that PLK-1 plays distinct roles in meiotic spindle assembly/stability, chromosome alignment and segregation, and polar body extrusion during meiosis I. Furthermore, by a combination of live imaging and biochemical analysis we identified the chromosomal recruitment mechanisms of PLK-1 during *C. elegans* oocyte meiosis. The spindle assembly checkpoint kinase BUB-1 directly recruits PLK-1 to the kinetochore and midbivalent while the chromosome arm population of PLK-1 depends on a direct interaction with the centromeric-associated protein CENP-C^{HCP-4}. We found that perturbing both BUB-1 and CENP-C^{HCP-4} recruitment of PLK-1 leads to severe meiotic defects, resulting in highly aneuploid oocytes. Overall, our results shed light on the roles played by PLK-1 during oocyte meiosis and provide a mechanistic understanding of PLK-1 targeting to meiotic chromosomes.

32 **INTRODUCTION**

33 Meiosis consists of two consecutive segregation events following DNA replication – in
34 meiosis I homologous chromosomes segregate, half of which are then removed in a polar
35 body, before the remaining sister chromatids segregate in meiosis II to produce haploid
36 gametes (Marston and Amon, 2004; Ohkura, 2015). Tight spatial and temporal control of
37 protein localisation and activity is required to ensure chromosome/chromatid alignment and
38 segregation occur efficiently and the correct number of chromosomes is present in each
39 gamete (Marston and Wassmann, 2017). Phosphorylation is a key post-translational
40 modification utilised to regulate protein localisation and activity, which is fundamentally
41 important for the success of both mitotic and meiotic cell divisions (Marston and Wassmann,
42 2017; Saurin, 2018). Therefore, the regulation of kinase or phosphatase localisation and
43 activity is vital for proper cell division, with the balance of their effects determining the
44 localisation/activity of substrate proteins that play important roles in the cell division process
45 (Gelens et al., 2018; Novak et al., 2010).

46 Polo-like kinases (PLKs) are a family of Ser/Thr protein kinases first discovered in
47 Drosophila (Llamazares et al., 1991; Sunkel and Glover, 1988) and yeast (Kitada et al., 1993;
48 Ohkura et al., 1995) and later findings showed that PLKs are present in all eukaryotes
49 (Zitouni et al., 2014). PLK1 is essential for meiotic and mitotic cell divisions, with its
50 localisation and functions proving well conserved throughout eukaryotic evolution. PLK-1
51 localises to the centrosomes, kinetochore, central spindle, and midbody during mitosis and is
52 involved in numerous processes including mitotic entry, spindle assembly, chromosome
53 alignment, the spindle assembly checkpoint, and cytokinesis (Archambault and Glover, 2009;
54 Petronczki et al., 2008; Schmucker and Sumara, 2014; Zitouni et al., 2014). During
55 mammalian meiosis, PLK-1 localises to the chromosomes and spindle poles in prometaphase
56 and metaphase. In anaphase PLK-1 is localised primarily in the central spindle between the

segregating chromosomes and then the midbody during polar body extrusion (Pahlavan et al., 2000; Solc et al., 2015; Tong et al., 2002; Wianny et al., 1998). Inhibition of PLK-1 in mammalian oocytes has indicated roles in many processes including germinal vesicle breakdown, spindle assembly, chromosome alignment, and polar body extrusion (Solc et al., 2015; Tong et al., 2002). To understand why PLK-1 is crucial for meiosis it is critical to characterise precisely where PLK-1 is located and how it is recruited to specific regions, which will allow further dissection of the discrete roles of PLK-1 during meiosis.

PLK-1 interacts with proteins via its C-terminal polo-binding domain (PBD) (Cheng, 2003; Elia et al., 2003a). The PBD binds to phosphorylated motifs of the consensus Ser-phSer/phThr-X, where ph indicates a phosphorylated residue and X indicates any amino acid (Elia et al., 2003a, 2003b). When X is a proline, phosphorylation of the central Ser/Thr residue is often mediated by a proline-directed kinase, notably Cdk1:Cyclin B during cell division (Elowe et al., 2007; Qi et al., 2006) - this motif will henceforth be termed STP motif. When a non-proline residue occupies position X, PLK-1 itself can phosphorylate the central Ser/Thr, thereby enhancing its own recruitment (Kang et al., 2006; Neef et al., 2003), referred to as self-priming. Furthermore, PLK-1 binding to STP motifs via the PBD induces a conformational change that enhances its kinase activity (Mundt et al., 1997; Xu et al., 2013). While the mechanism of PLK-1 recruitment to the chromosomes during oocyte meiosis has not been characterised, recruitment of PLK-1 to the kinetochore during mammalian mitosis has been investigated. In mammals, the constitutive centromere-associated network (CCAN) complex of proteins binds to the histone variant CENP-A at centromeres (Foltz et al., 2006; Izuta et al., 2006; Okada et al., 2006). Outer kinetochore proteins bind to the CCAN and ultimately mediate chromosome alignment and segregation via interaction with microtubules (Musacchio and Desai, 2017). Two proteins are primarily responsible for PLK-1 recruitment to the kinetochore – CCAN component CENP-U (Kang et al., 2011, 2006; Singh et al., 2021)

82 and the spindle assembly checkpoint kinase BUB-1 (Elowe et al., 2007; Qi et al., 2006; Singh
83 et al., 2021), both of which directly bind to PLK-1 via STP motifs in a Cdk1-dependent
84 manner.
85 In *C. elegans,* PLK-1 localisation in meiosis and mitosis is similar to other organisms (Chase
86 et al., 2000). In mitosis, roles of PLK-1 include nuclear envelope breakdown (NEBD)
87 (Martino et al., 2017), merge of parental genomes in the embryo through lamina disassembly
88 (Rahman et al., 2015; Velez-Aguilera et al., 2020), centrosome maturation (Cabral et al.,
89 2019; Decker et al., 2011; Ohta et al., 2021; Woodruff et al., 2015), and cytokinesis (Gómez-
90 Cavazos et al., 2020) – indicating that major mitotic roles of PLK-1 are conserved in *C.*
91 *elegans.* However, meiotic roles of PLK-1 in *C. elegans* oocytes have remained obscure, as
92 PLK-1 depletion results in severely defective NEBD and oocytes with a whole nucleus rather
93 than condensed chromosomes (Chase et al., 2000). In the PLK-1-depleted oocytes that
94 'escaped' the NEBD defect, chromosome congression, segregation, and polar body extrusion
95 were severely disrupted. However it is unclear whether these phenotypes are indirect effects
96 of the severe early meiotic defects or whether they result from specific functions of PLK-1
97 throughout meiosis (Chase et al., 2000). Furthermore, while PLK-1 was shown to localise
98 broadly to chromosomes and the spindle during meiosis (Chase et al., 2000), a more precise
99 dynamic characterisation of PLK-1 localisation during meiosis is lacking.
100 Here, by temporally inhibiting an analogue-sensitive PLK-1 mutant we show that PLK-1 is
101 involved in spindle assembly/stability, chromosome alignment and segregation, and polar
102 body extrusion in *C. elegans* oocytes. Using live imaging and immunofluorescence, we find
103 that PLK-1 localises to the spindle poles, chromosome arms, kinetochores, and midbivalent
104 region between the homologous chromosomes during meiosis I in *C. elegans* oocytes. By a
105 combination of live imaging and *in vitro* biochemical analysis, we have characterised the full
106 chromosomal recruitment mechanisms of PLK-1 during meiosis – showing that CENP-C^{HCP-4}

107 directly recruits PLK-1 to the chromosome arms while PLK-1 recruitment to the midbivalent
108 and kinetochore is mediated by a direct interaction with BUB-1. Furthermore, BUB-1- and
109 CENP-C-mediated PLK-1 recruitment to chromosomes is essential for meiosis I.

110 **RESULTS**

111 **PLK-1 plays roles in spindle stability, chromosome alignment, segregation, and polar**
112 **body extrusion in meiosis I**

113 A previous study showed that PLK-1 localises to the meiotic spindle and chromosomes in *C.*
114 *elegans* oocytes and depletion of PLK-1 using RNAi led to several defects including defective
115 NEBD, chromosome segregation, and polar body extrusion (Chase et al., 2000). While this
116 suggested that PLK-1 plays several roles during meiosis, the use of RNAi presents a
117 limitation to addressing them independently. In particular, the strong NEBD defect
118 complicates delineation of the roles of PLK-1 at later stages of meiosis. Therefore, we sought
119 to understand the distinct localisation and roles of PLK-1 during meiosis I.

120 To assess PLK-1 localisation during meiosis with high spatial and temporal resolution, we
121 imaged endogenously tagged sfGFP::PLK-1 in dissected oocytes. PLK-1 localises to the
122 spindle poles (Figure 1A-C; blue arrows), chromosome arms (Figure 1A-C; yellow arrows),
123 and midbivalent region between the homologous chromosomes during Prometaphase I
124 (Figure 1A-C; magenta arrow). This localisation pattern was confirmed with immunostaining
125 of fixed oocytes using a specific anti-PLK-1 antibody (Figure 1D). As chromosomes begin to
126 segregate in early anaphase, PLK-1 is mostly observed on chromosomes and, to a lesser
127 extent, in between the segregating chromosome masses (Figure 1B, yellow and magenta
128 arrows, respectively; see also Figure S1). During late anaphase, PLK-1 is still detectable on
129 chromosomes, and is enriched in the central spindle (Figure 1B, green arrow; see also Figure
130 S1).

131 Since long-term depletion of PLK-1 leads to severe NEBD defects (Chase et al., 2000, Figure
132 1E), we used an analogue-sensitive *plk-1* allele (Gómez-Cavazos et al., 2020; Woodruff et al.,
133 2015) that renders it sensitive to chemically modified derivatives of PP1, a Src family
134 inhibitor (Bishop et al., 2000). We reasoned that acute PLK-1as inhibition for a short period of

135 time would allow us to study the post-NEBD effects (Figure 1E). We tested a variety of
136 analogues and all of them led to embryonic lethality of the *plk-1*^{as} strain without affecting a
137 wild type strain (Figure S2). We decided to continue our experiments with the 3-substituted
138 benzyl PP1 derivative 3IB-PP1, which showed the best specificity and potency (Figure S2). A
139 wild type strain in the presence of 3IB-PP1 and *plk-1*^{as} in the presence of vehicle control
140 ('EtOH') behaved normally during meiosis (Figure 1F,G & Figure S3). Addition of 10 μM
141 3IB-PP1 between 5 and 15 min before dissection and imaging of oocytes allowed us to bypass
142 the NEBD defect and 6 bivalents were easily identifiable within the newly fertilised oocyte
143 (Figure 1F, yellow arrows). Under these conditions PLK-1as inhibition led to drastic spindle
144 defects with no observable bipolar spindle formation and no consequent chromosome
145 segregation was observed, indicating that PLK-1 is involved in spindle assembly and/or
146 stability during oocyte meiosis (Figure 1F). We sought to minimise the spindle defects upon
147 PLK-1 inhibition by reducing the concentration of 3IB-PP1 to 0.1-1 μM and omitting the pre-
148 treatment step prior to dissection. Under these conditions, ~62% of oocytes had seemingly
149 bipolar spindles and chromosomes remained somewhat associated with the spindle, although
150 chromosome alignment was still affected in 56% of oocytes (≥2 misaligned chromosomes,
151 Figure 1G,H). A more detailed analysis of chromosome dynamics after PLK-1 inhibition is
152 presented in Figure S3, where individual chromosomes are followed every 20 seconds and, as
153 opposed to wild type, chromosomes from PLK-1-inhibited oocytes show a highly dynamic
154 behaviour whereby they seem to briefly align and then become misaligned again (Figure
155 S3A,B and arrows therein). We then used the pole marker ASPM-1 to allow proper
156 characterisation of spindle bipolarity under these conditions and confirmed that even when
157 two ASPM-1 poles are clearly discerned (Figure 1I, blue arrows), chromosome alignment
158 fails (Figure 1I, yellow arrows). Hence, it appears that PLK-1 participates in chromosome

159 alignment in a manner that is at least partially independent of its roles in overall spindle
160 assembly/stability.
161

162 **BUB-1 recruits PLK-1 to the midbivalent during oocyte meiosis**

163 To further understand the role of PLK-1 during meiosis, we sought to identify the PLK-1
164 recruitment mechanism(s). In mammalian mitosis, the kinase BUB-1 and its paralog BUBR1
165 directly recruit PLK-1 to the kinetochore via STP motifs that are phosphorylated by Cdk1
166 (Elowe et al., 2007; Qi et al., 2006). While the *C. elegans* BUBR1 ortholog MAD3^{SAN-1} does
167 not localise to the chromosomes or spindle during meiosis (Bel Borja et al., 2020), BUB-1
168 localises to the kinetochores and midbivalent region (Dumont et al., 2010; Monen et al., 2005;
169 Pelisch et al., 2019, 2017). We investigated whether BUB-1 was involved in PLK-1 targeting
170 during *C. elegans* meiosis. RNAi-mediated depletion of BUB-1 led to the loss of PLK-1 from
171 the midbivalent (Figure 2A,B; blue arrows). In contrast, PLK-1 signal at chromosome arms
172 remained unaffected and what appeared to be a pole signal was also detected (Figure 2A,B;
173 yellow and green arrows, respectively). Analysis of the BUB-1 protein sequence revealed a
174 putative polo-docking STP motif in amino-acids 526-528 that is conserved in nematode
175 species (Figure 2C). Therefore, we sought to identify whether *C. elegans* BUB-1 directly
176 interacts with PLK-1 to mediate its recruitment to the midbivalent region.
177

178 **BUB-1 directly interacts with PLK-1 through a Cdk1-dependent STP motif**

179 To test whether BUB-1 directly interacts with PLK-1 *in vitro*, we purified a recombinant
180 fragment of BUB-1 encompassing the intrinsically disordered region between the TPR and
181 kinase domains that contains the putative STP motif ('BUB-1$^{190-628}$'). Since the interaction
182 between STP motifs and the PBD of PLK-1 requires phosphorylation of the central Ser/Thr
183 residue (Elia et al., 2003a, 2003b), we conducted kinase assays to assess the phosphorylation

184 of BUB-1$^{190-628}$. Cdk1 and PLK-1 can both phosphorylate BUB-1$^{190-628}$ (Figure S4A,B).
185 Interestingly, kinase assays conducted with Cdk1 and PLK-1 together produced a prominent
186 shifted band representing phosphorylated protein that was not present with the individual
187 kinases (Figure 2D). Since STP motifs are known to be targets of proline-directed kinases
188 such as Cdk1 (Elowe et al., 2007; Qi et al., 2006), we hypothesised that Cdk1 phosphorylates
189 the central threonine of the STP motif (T527), allowing PLK-1 to bind directly to BUB-1
190 resulting in the shifted band representing highly phosphorylated BUB-1. To test this
191 hypothesis, we mutated T527 in the STP motif to alanine ('BUB-1$^{190-628}$(T527A)') and
192 assessed the resulting phosphorylation using the phosphoprotein stain Pro-Q^{TM} Diamond.
193 T527A mutation in BUB-1$^{190-628}$ largely prevented the shift observed in the combined Cdk1
194 and PLK-1 assay (Figure 2E), indicating that phosphorylation of this residue is essential for
195 the shifted band observed when Cdk1 and PLK-1 both phosphorylate BUB-1$^{190-628}$.
196 To determine whether BUB-1 directly binds to PLK-1, we purified a maltose-binding protein
197 (MBP)-tagged PLK1 PBD (MBP-PLK1^{PBD}) (Singh et al., 2021) and incubated it with
198 unphosphorylated or Cdk1-phosphorylated BUB-1$^{190-628}$ before assessing complex formation
199 by size-exclusion chromatography (SEC). Cdk1-phosphorylated BUB-1 formed a stable
200 complex with MBP-PLK1^{PBD} (Figure 2F). While unphosphorylated BUB-1 showed some
201 interaction with MBP-PLK1^{PBD}, this complex eluted from the column at a higher volume and
202 bound to a lower proportion of the MBP-PLK1^{PBD}, suggestive of a weaker interaction and/or
203 different stoichiometry (Figure 2F). To directly test whether phosphorylation of T527 is
204 required for PLK-1 to bind to BUB-1, MBP-PLK1^{PBD} was incubated with Cdk1-
205 phosphorylated BUB-1$^{190-628}$ or BUB-1$^{190-628}$(T527A) and SEC was used to assess complex
206 formation again. Interestingly, when Cdk1-phosphorylated BUB-1$^{190-628}$(T527A) was
207 incubated with MBP-PLK1^{PBD}, the resulting elution was reminiscent of the unphosphorylated
208 wild type BUB-1$^{190-628}$ (Figures 2G). Together, these data indicate that there is a Cdk1

209 phosphorylation-dependent interaction between BUB-1 and PLK1^{PBD} that requires
210 phosphorylation of T527 within the STP motif of BUB-1. To further confirm that the STP
211 motif of BUB-1 can interact with the PBD in a T527 phosphorylation-dependent manner,
212 fluorescence polarisation assays were conducted using FITC-labelled peptides containing the
213 BUB-1 STP motif (Figure 2H). The phosphorylated STP motif bound to MBP-PLK1^{PBD} with
214 high affinity (K_D below 100 nM) while the unphosphorylated peptide did not interact with
215 MBP-PLK1^{PBD} at the concentrations tested (Figure 2H).
216 Altogether, these data indicate that *C. elegans* BUB-1 can directly bind to PLK-1 *in vitro* in a
217 phospho-dependent manner via a newly characterised STP motif.
218
219 **BUB-1 directly recruits PLK-1 to the midbivalent in vivo**
220 We then sought to determine whether the STP motif in BUB-1 is responsible for PLK-1
221 recruitment *in vivo.* Using CRISPR-Cas9, we generated the T527A mutation in the
222 endogenous *bub-1* locus (*bub-1^{T527A}*). *bub-1^{T527A}* mutant worms showed significant embryonic
223 and larval lethality so we generated a balanced strain in which the *bub-1^{T527A}* allele was
224 maintained as a heterozygote. Homozygous *bub-1^{T527A}* worms from heterozygous parents
225 develop to adulthood and produce oocytes that go through meiosis, which allowed us to study
226 the role of the STP motif in BUB-1 during meiosis. PLK-1 was absent from the midbivalent
227 in *bub-1^{T527A}* oocytes, reminiscent of the *bub-1(RNAi)* phenotype (Figure 3A, blue arrowheads
228 and 3B). Importantly, BUB-1 localisation to the midbivalent and kinetochore was maintained
229 in the *bub-1^{T527A}* strain (Figure 3C), indicating that BUB-1 directly interacts with PLK-1 via
230 this STP motif *in vivo* to recruit PLK-1 to the midbivalent. To assess the impact of BUB-1
231 mediated PLK-1 recruitment during meiosis I, we crossed the *bub-1^{T527A}* allele with a strain
232 expressing GFP-tagged tubulin and mCherry-tagged histone and analysed chromosome
233 alignment, segregation, and polar body extrusion defects (See Methods). *bub-1^{T527A}* mutant

234 oocytes displayed chromosome alignment defects in ~62% of the oocytes, with 32% of
235 oocytes showing severe alignment defects (Figure 3D,E). Additionally, ~1/4 of *bub-1*^{T527A}
236 oocytes showed mild anaphase defects (Figure 3E). Despite these defects, more than 90% of
237 *bub-1*^{T527A} oocytes show visible separation of two chromosome masses and polar body
238 extrusion occurred normally at the end of meiosis I (Figure 3E).
239 Overall, our results show that an STP motif in BUB-1 directly recruits PLK-1 to the
240 midbivalent during meiosis I and this interaction is primarily important for chromosome
241 alignment.
242
243 **CENP-C^{HCP-4} recruits PLK-1 to meiotic chromosome arms**
244 PLK-1 localisation to chromosome arms remained unchanged when BUB-1 was depleted
245 (Figure 2A,B) or the STP motif was mutated (Figure 3A,B), indicating that a different
246 pathway is required to recruit this population of PLK-1. We therefore sought to identify the
247 mechanism of PLK-1 recruitment to the chromosome arms. In mammalian mitosis, PLK-1
248 recruitment to the kinetochore is mediated by BUB-1 and CCAN component CENP-U (Elowe
249 et al., 2007; Kang et al., 2011, 2006; Qi et al., 2006; Singh et al., 2021). Interestingly, the
250 CCAN appears to be largely absent in *C. elegans* (Maddox et al., 2012), and kinetochore
251 assembly depends on the CENP-C orthologue, HCP-4 (hereafter CENP-C^{HCP-4}) during mitosis
252 (Oegema et al., 2001) and on CENP-C^{HCP-4} and the nucleoporin ELYS^{MEL-28} during meiosis
253 (Hattersley et al., 2022). CENP-C^{HCP-4} localises to chromosomes throughout meiosis I (Figure
254 4A) (Hattersley et al., 2022; Monen et al., 2005). Like its mammalian counterpart, CENP-
255 C^{HCP-4} is predicted to be mostly disordered and it contains a putative N-terminal STP motif
256 encompassing amino acids 162-164 that is conserved in nematode species (Figure 4B).
257 Although CENP-C^{HCP-4} depletion does not have a major impact on meiosis I (Hattersley et al.,
258 2022; Monen et al., 2005), RNAi-mediated depletion of CENP-C^{HCP-4} abolished PLK-1

259 localisation on chromosome arms (Figure 4C,D). PLK-1 is still present in the midbivalent
260 (Figure 4C,D, blue arrows) which suggests that BUB-1 and CENP-C^{HCP-4} represent
261 independent pathways for PLK-1 targeting. Additionally, CENP-C^{HCP-4} depletion revealed a
262 pool of PLK-1 which is kinetochore-associated (Figure 4C,D, yellow arrows). Since the
263 above data indicated that CENP-C^{HCP-4} is involved in PLK-1 recruitment to chromosome
264 arms, we sought to determine whether this involved a direct interaction via the putative STP
265 motif identified in sequence alignments.
266

267 **CENP-C^{HCP-4} interacts directly with PLK-1 through a Cdk1-dependent STP motif**

268 To investigate whether CENP-C^{HCP-4} directly interacts with PLK-1, we purified a recombinant
269 N-terminal fragment of CENP-C^{HCP-4} ('CENP-C$^{HCP-4(1-214)}$'). As the putative CENP-C^{HCP-4}
270 STP motif also contains a proline-directed kinase consensus site, we assessed Cdk1
271 phosphorylation of the recombinant fragment. Cdk1 kinase assays showed that CENP-C^{HCP-}
272 $^{4(1-214)}$ can be phosphorylated by Cdk1 and mutation of the putative STP motif threonine to
273 alanine (T163A) reduced the phosphorylation of the fragment (Figure 5A). To determine
274 whether this putative STP motif directly binds to PLK-1 in a Cdk1-dependent manner, we
275 used size exclusion chromatography. Cdk1-phosphorylated CENP-C$^{HCP-4(1-214)}$ forms a stable
276 complex with MBP-PLK1^{PBD}, while the unphosphorylated protein did not (Figure S5). We
277 then tested the requirement of T163 phosphorylation on CENP-C$^{HCP-4(1-214)}$ to interact with
278 MBP-PLK1^{PBD}. Phosphorylated wild type CENP-C$^{HCP-4(1-214)}$ forms a stable complex with
279 MBP-PLK1^{PBD}; on the contrary, phosphorylated CENP-C$^{HCP-4(1-214)}$ (T163A) did not form a
280 stable complex with MBP-PLK1^{PBD} (Figure 5B). Together, these data indicate that CENP-
281 C$^{HCP-4(1-214)}$ phosphorylated by Cdk1 can bind to the PBD and this interaction requires
282 phosphorylation of T163 within the STP motif. To further confirm this STP motif binds to
283 MBP-PLK-1^{PBD} in a phospho-dependent manner, we conducted fluorescence polarisation

284 assays with FITC-labelled CENP-C^{HCP-4} STP motif peptides. The Thr 163 phosphorylated
285 peptide bound to MBP-PLK1^{PBD} with high affinity (K_D in the low hundreds nM), while the
286 unphosphorylated peptide did not display binding at the concentrations indicated (Figure 5C).
287 Collectively, these data indicate that the putative STP motif in CENP-C^{HCP-4} binds to the
288 PBDs of PLK1 in a Cdk1 phosphorylation-dependent manner, which led us to assess the
289 importance of this STP motif *in vivo*.
290

291 **CENP-C^{HCP-4} recruits PLK-1 to chromosome arms in vivo through an STP motif**

292 The T163A mutation in CENP-C^{HCP-4} was generated in the endogenous *hcp-4* locus (*hcp-*
293 *4^{T163A})* which, unlike *bub-1^{T527A},* did not affect viability. When GFP:PLK-1 was monitored in
294 dissected oocytes, *hcp-4^{T163A}* recapitulated the full CENP-C^{HCP-4} depletion with PLK-1
295 localising only to the midbivalent and kinetochore but absent from chromosome arms (Figure
296 5D,E). This indicates that PLK-1 is targeted to chromosome arms directly through the
297 phospho-dependent STP motif in CENP-C^{HCP-4}. Importantly, CENP-C^{HCP-4}(T163A) displays
298 an indistinguishable localisation from wild type CENP-C^{HCP-4} (Figure 5F) and the other PLK-
299 1 receptor, BUB-1, also localises normally in the *hcp-4^{T163A}* strain (Figure 5G).
300 These data indicate that CENP-C^{HCP-4} directly recruits PLK-1 to the chromosome arms during
301 meiosis I via a newly characterised N-terminal STP motif.
302

303 **Dual PLK-1 recruitment by BUB-1 and CENP-C is essential for meiosis I**

304 Our results so far indicate that PLK-1 recruitment to the midbivalent during meiosis I is
305 mediated by direct interaction with BUB-1, while PLK-1 localisation to the chromosome
306 arms requires direct interaction with CENP-C^{HCP-4}. Co-depletion of BUB-1 and CENP-C^{HCP-4}
307 by RNAi led to complete absence of PLK-1 at the chromosome arms, midbivalent, and
308 kinetochore (Figure 6A). This confirmed that the BUB-1 and CENP-C^{HCP-4} pathways are the

309 primary recruiters of PLK-1 to the chromosomes during oocyte meiosis. Additionally, the
310 kinetochore population of PLK-1 was lost when BUB-1 and HCP-4 were co-depleted,
311 indicating that BUB-1 is responsible for recruiting PLK-1 to the kinetochore as well as the
312 midbivalent (Figure 6A). RNAi of BUB-1 causes significant defects in spindle stability,
313 chromosome alignment, and chromosome segregation during meiosis (Dumont et al., 2010;
314 Pelisch et al., 2019). However, co-depletion of BUB-1 and CENP-C^{HCP-4} exacerbated the
315 chromosome alignment and segregation errors and resulted in a significantly higher
316 proportion of polar body extrusion failures (Figure 6B-C). Therefore, while CENP-C^{HCP-4}
317 depletion does not have noticeable defects on its own, it enhances the BUB-1 depletion
318 phenotype. To focus more specifically on the effects of direct PLK-1 recruitment, we depleted
319 CENP-C^{HCP-4} in *bub-1*^{T527A} mutant oocytes. This abolished PLK-1 localisation in the same
320 manner as co-depletion of BUB-1 and CENP-C^{HCP-4} (Figure 6D) as well as displaying defects
321 in chromosome alignment, segregation, and polar body extrusion of a greater severity than
322 *hcp-4(RNAi)* or *bub-1*^{T527A} alone (Figure 6E,F). Similar results were obtained when
323 performing the complementary experiment using *hcp-4*^{T163A}/*bub-1(RNAi)* oocytes (Figure S6).
324 These data indicate that recruitment of PLK-1 to the midbivalent and kinetochore by BUB-1
325 appears to be primarily responsible for the chromosomal roles of PLK-1 during meiosis I, as
326 disruption of this pathway leads to meiotic defects while perturbing CENP-C^{HCP-4} recruitment
327 of PLK-1 on its own does not. However, the fact that disruption of both BUB-1 and CENP-
328 C^{HCP-4} recruitment pathways enhances the severity of the resulting meiotic defects indicates
329 that the CENP-C^{HPC-4} pathway does still play an active part in the roles of PLK-1 during
330 meiosis I.
331
332

333 **DISCUSION**

334 In the present manuscript we describe specific, post-NEBD roles played by PLK-1 during
335 oocyte meiosis. PLK-1 is important for spindle assembly/stability, chromosome alignment
336 and segregation, and polar body extrusion during meiosis I. We found that PLK-1 localises to
337 spindle poles and chromosomes during metaphase I before localising to the chromosomes and
338 central spindle in anaphase. Furthermore, we characterised the mechanisms of chromosomal
339 PLK-1 targeting during oocyte meiosis, which rely on the centromere-associated protein
340 CENP-C^{HCP-4} and the spindle assembly checkpoint kinase BUB-1. While CENP-C^{HCP-4}
341 targets PLK-1 to chromosome arms, BUB-1 directs PLK-1 to the midbivalent and
342 kinetochores. In both cases, interaction with PLK-1 relies on phosphorylated STP motifs
343 within predicted disordered regions. While we have not confirmed that these sites are
344 phosphorylated by Cdk1 *in vivo,* several lines of evidence indicate this is likely the case: 1)
345 both motifs have Pro at position 3, indicative of potential proline-directed kinase substrates;
346 2) Cdk1 is the most prominent proline-directed kinase in cell division and known to
347 phosphorylate STP motifs, including that of mammalian BUB-1 (Qi et al., 2006); 3) both sites
348 were phosphorylated by Cdk1, but not PLK-1, *in vitro*; and 4) fluorescence polarisation
349 experiments indicate that phosphorylation of the Thr residues within the STP motifs is
350 essential for the interaction with the PBD, clearly displaying why the alanine mutants have
351 such a drastic effect on PLK-1 localisation *in vivo*. We found that mutating the STP motif in
352 BUB-1 results primarily in chromosome alignment defects. While disrupting the CENP-C^{HCP-}
353 ^{4}-mediated localisation of PLK-1 to the chromosome arms does not have a significant
354 phenotypic defect on its own, it does enhance the meiotic defects observed when the BUB-1-
355 dependent kinetochore and midbivalent populations are disrupted. This suggests that while
356 BUB-1 recruitment of PLK-1 may mediate the most important functions of PLK-1 during

357 meiosis I, CENP-C^{HCP-4} recruitment of PLK-1 to the chromosome arms also plays an active
358 role in meiosis.
359
360 **Expanding on the meiotic roles of PLK-1**
361 By temporally inhibiting an analogue-sensitive PLK-1 mutant during *C. elegans* oocyte
362 meiosis, we have shown that PLK-1 plays a major role in the regulation of the meiotic
363 spindle. At high concentrations of analogue this resulted in the complete lack of spindle
364 bipolarity, and even at low concentrations the majority of oocytes (62%) imaged lacked an
365 apparent bipolar spindle. While this clearly displays a key role of PLK-1 during meiosis is in
366 the regulation of the meiotic spindle, we cannot distinguish more specific mechanisms using
367 our experimental techniques. As a result, we have characterised the phenotype as a lack of
368 spindle stability throughout this manuscript, but it should be noted that we cannot distinguish
369 whether these effects are on the spindle assembly process itself or on the maintenance of an
370 assembled bipolar spindle. Potential mechanisms of meiotic spindle regulation by PLK-1
371 include the microtubule depolymerase KLP-7, the *C. elegans* ortholog of the MCAK/Kinesin
372 13 family. There is some evidence to indicate that PLK-1 may regulate the kinesin 13
373 microtubule depolymerases in other organisms (Jang et al., 2009; Ritter et al., 2014; Sanhaji
374 et al., 2014; Shao et al., 2015; Zhang et al., 2011) and KLP-7 localises to the chromosomes,
375 during meiosis I (Connolly et al., 2015; Danlasky et al., 2020; Gigant et al., 2017; Han et al.,
376 2015), which overlaps with PLK-1 localisation. Furthermore, disrupting KLP-7 function
377 prevents proper bipolar spindle assembly and results in microtubules protruding out of the
378 meiotic spindle towards the cytoplasm (Connolly et al., 2015; Gigant et al., 2017), two
379 phenotypes we also see with PLK-1 inhibition.
380 Aside from the large-scale spindle defects observed when PLK-1 is inhibited, chromosome
381 alignment is still disrupted when the structure of the spindle appears bipolar and largely

382 normal. Since the mechanism of chromosome alignment by acentrosomal meiotic spindles is
383 not as well characterised as the centrosomal mitotic equivalent, speculating on the
384 underpinning mechanisms of this phenotype is challenging. However, it should be noted that
385 we cannot exclude the possibility that this phenotype is also a direct result of the dysregulated
386 spindle upon PLK-1 inhibition. Indeed, there is some evidence to suggest that a chromosome-
387 dependent pathway of microtubule formation may be an important aspect of chromosome
388 alignment and segregation (Conway et al., 2022; Heald et al., 1996; Kiewisz et al., 2022).
389 Despite these specific hypotheses mentioned above, it is clear that there will be many
390 different proteins and pathways impacted by PLK-1 phosphorylation throughout meiosis I
391 that will ultimately contribute to the severe defects we observe upon PLK-1 inhibition. While
392 a focussed investigation into specific hypotheses would no doubt yield important results, an
393 unbiased approach to identify the relevant PLK-1 substrates during meiosis would be
394 particularly useful for investigation of the key effects of PLK-1 during meiosis. There are
395 obvious technical challenges to overcome before this can be achieved, not least of which
396 would be isolating a large enough sample of meiotic oocytes to perform robust quantitative
397 proteomics. The work in this manuscript undertaken to identify the mechanisms of PLK-1
398 targeting during oocyte meiosis I will be instrumental for a later characterisation of the
399 localisation and meiotic stage-specific analysis of PLK-1 substrates.
400

401 **Comparison with dual recruitment in mammals (CENP-U vs CENP-C)**

402 During mammalian mitosis, PLK1 is recruited to kinetochores through BUB1 and CENP-U,
403 relying on self-priming in addition to Cdk1-mediated priming (Kang et al., 2011, 2006; Qi et
404 al., 2006; Singh et al., 2021). Our results suggest that Cdk1-mediated priming is the primary
405 mechanism for PLK-1 recruitment in both BUB-1- and CENP-C-dependent branches.
406 Additionally, we noted the presence of a putative B56 short linear motif (LxxIxE) 38 aa

407 downstream of the STP motif in *C. elegans* CENP-C (203-IPTILE-208). This is relevant
408 because it has been shown that PLK1 and B56 motifs tend to co-exist in close proximity
409 (Cordeiro et al., 2020; Singh et al., 2021). This makes a putative cross-talk between PLK-1
410 and PP2A/B56 a worthy avenue to follow-up on our current findings.
411 Apparent lack of a CCAN network along with retention of crucial roles for PLK1 in species
412 like *C. elegans* and *Drosophila melanogaster* (*D. melanogaster*) suggest that the CENP-U
413 pathway could have been replaced by other proteins. CENP-C is a good candidate, as the only
414 CCAN component in these species. While we confirm that this is the case in *C. elegans*, it is
415 interesting to note that putative STPs exist in sequences 176-178 and 266-268 in *D.*
416 *melanogaster* CENP-C (Uniprot #Q9VHP9). Interestingly, *D. melanogaster* Polo and CENP-
417 C co-localise and this co-localisation increases by ectopic centromere generation through
418 CENP-A (CID) over-expression (Heun et al., 2006).
419
420 Overall, our results advance our understanding on the roles played by PLK-1 during oocyte
421 meiosis and provide a mechanistic understanding of PLK-1 targeting to meiotic
422 chromosomes. The next step will be to identify and characterise PLK-1 meiotic substrates, to
423 understand exactly how PLK-1 participates in each of its meiotic roles.
424
425
426
427
428

ACKNOWLEDGEMENTS

We thank Arshad Desai for sharing strains and antibodies and for helpful discussions and sharing results prior to publication; Pierre Gönczy for the PLK-1 antibody; Lionel Pintard for providing PLK-1 for the initial experiments and the plasmid for expression and purification; Bruce Bowerman for the GFP::ASPM-1 strain; Satpal Virdee for advice on fluorescence polarisation experiments. We also thank Ron Hay for comments on the manuscript. This work was supported by a Career Development Award from the Medical Research Council (grant MR/R008574/1) and an ISSF grant funded by the Wellcome Trust (105606/Z/14/Z). ST is funded by a Medical Research Council Doctoral Training Programme. DKC is supported by a Sir Henry Dale Fellowship from the Wellcome Trust (208833). We acknowledge the FingerPrints Proteomics Facility and the Dundee Imaging Facility, which are supported by a 'Wellcome Trust Technology Platform' award (097945/B/11/Z) and the Tissue Imaging Facility, funded by a Wellcome Trust award (101468/Z/13/Z). Some nematode strains were provided by the CGC, which is funded by NIH Office of Research Infrastructure Programs (P40 OD010440).

AUTHOR CONTRIBUTIONS

S.J.P.T. designed, performed and analysed experiments, and wrote the manuscript.

L.B-B. designed, performed and analysed experiments.

F.S. designed, performed and analysed experiments.

D.C. generated novel reagents (nematode strains).

F.P. designed, performed and analysed experiments; acquired funding; wrote the manuscript.

451 **FIGURE LEGENDS**

452

453 **Figure 1. Analysis of PLK-1 localisation and inhibition during meiosis I.**

454

455 A) Schematic of a *C. elegans* bivalent, highlighting the midbivalent and kinetochore.

456 B) *In situ* GFP-tagged PLK-1 (Martino et al., 2017) was followed through meiosis I in

457 live, dissected oocytes. Scale bar, 2 µm. More detailed sequence of events are

458 displayed in Figure S1. Yellow arrows point to chromosomes, blue arrows indicate

459 spindle poles, magenta arrows point towards the midbivalent, and green arrow

460 indicates the central spindle.

461 C) Line profile analysis of PLK-1::GFP during early Metaphase I, as indicated by the

462 yellow line in B). Background signal was subtracted and maximum signal for each

463 channel was set to 1.

464 D) Immunostaining of (untagged) PLK-1 in fixed oocytes. The insets represent a

465 magnified image of single bivalents for each channel.

466 E) Schematic of the last two maturing oocytes and the fertilised egg, highlighting the

467 difference between PLK-1 depletion and acute PLK-1 inhibition.

468 F) *plk-1*^{as} worms expressing GFP-tagged tubulin and mCherry-tagged histone were

469 dissected in medium containing ethanol ('EtOH', control) or the PP1 analogue 3IB-

470 PP1 (10 µM). Yellow arrows point to the each of the six bivalents. Scale bar, 2 µm.

471 G) *plk-1*^{as} worms expressing GFP-tagged tubulin and mCherry-tagged histone, were

472 dissected in medium containing ethanol ('EtOH', control) or 0.1 µM PP1 analogue

473 3IB-PP1. Scale bar, 2 µm. The panels on the right show specific Z slices to highlight

474 individual chromosomes. Yellow arrows point to misaligned chromosomes contained

475 within the spindle, whereas blue arrows indicate chromosomes outside the spindle.
476 See also Figure S3.
477 H) Chromosme alignmend defects scored for 0.1-1 µM 3IB-PP1-treated oocytes are
478 presented in the graph.
479 I) Worms expressing GFP-tagged ASPM-1 (pole marker) and mCherry-tagged histone
480 along with analogue-sensitive *plk-1*, were dissected in medium containing ethanol
481 ('EtOH', control) or the PP1 analogue 3IB-PP1 at 1 µM or 10 µM. Scale bar, 2 µm.
482 Early metaphase I spindles are shown for each condition.
483
484 **Figure 2. BUB-1 regulates PLK-1 localisation in vivo and directly binds to PLK-1 *in***
485 ***vitro*.**
486
487 A) Control (*'wild type'*) and BUB-1 depleted ['*bub-1(RNAi)'*] oocytes expressing sfGFP-
488 tagged PLK-1 (and mCherry-tagged histone) were dissected and recorded throughout
489 meiosis I. Prometaphase/Metphase I is shown (before spindle rotation/shortening).
490 The yellow arrows indicate the bivalent chosen for magnification in each condition.
491 The blue arrows point to the midbivalent and the green arrow points to the spindle
492 pole. Left scale bar, 2 µm. Right scale bar, 1 µm.
493 B) Line profile analysis of PLK-1::GFP during early Metaphase I in *wild type* and *bub-*
494 *1(RNAi)* oocytes, as indicated by the yellow lines. Background signal was subtracted
495 and maximum signal for each channel was set to 1. Blue arrow points to the position
496 of the midbivalent.
497 C) Schematic representation of the *C. elegans* BUB-1 protein (top), sequence alignment
498 of the putative STP motif in nematode species (bottom).

499 D) Kinase assay of recombinant BUB-1$^{190-628}$ with Cdk1:Cyclin B, PLK-1, and both
500 kinases combined as indicated. Phosphorylation was assessed using SDS-PAGE
501 followed by coomassie (total protein) or ProQ diamond (phosphoprotein) staining.
502 E) Kinase assay of recombinant BUB-1$^{190-628}$ and BUB-1$^{190-628}$(T527A) with Cdk1:Cyclin
503 B and PLK-1 combined. Proteins were incubated with the kinases for the indicated
504 time points before phosphorylation was assessed by SDS-PAGE and staining with
505 either coomassie (total protein) or ProQ diamond (phosphoprotein).
506 F) Elution profile and coomassie-stained SDS-PAGE gels of representative fractions
507 from the Superdex 200 10/300 SEC column. BUB-1$^{190-628}$ was incubated with MBP-
508 PLK1^{PBD} at equimolar concentrations before separation by SEC. Binding was
509 conducted with unphosphorylated or Cdk1:Cyclin B phosphorylated BUB-1$^{190-628}$ as
510 indicated.
511 G) Elution profile and coomassie-stained SDS-PAGE gels of representative fractions
512 from the Superdex 200 10/300 SEC column. Wild type or T527A mutant BUB-1$^{190-628}$
513 was phosphorylated by Cdk1:Cyclin B before incubation with an equimolar
514 concentration of MBP-PLK1^{PBD}, binding was assessed by SEC.
515 H) FITC-labelled peptides containing the BUB-1 STP motif were incubated with
516 increasing concentrations of MBP:PLK1^{PBD} and binding analysed by fluoresence
517 polarisation. Unphosphorylated versus T527-phosphorylated peptides were compared.
518 'T^{Ph}' denotes phosphorylated Threonine.
519
520 **Figure 3. The polo-docking site in BUB-1 is required for PLK-1 targeting and**
521 **chromosome alignment.**
522

523 A) Fixed oocytes were stained with a PLK-1 specific antibody (green) and *bub-1*^{T527A}
524 heterozygote and homozygote oocytes were compared. DNA is shown in magenta.
525 The yellow arrow points to the midbivalent magnified on the right in each case and the
526 blue arrowhead points to the midbivalent.
527 B) Line profile analysis of PLK-1 localisation in fixed oocytes during early Metaphase I
528 in *bub-1*^{T527A} heterozygote ('*bub-1*^{T527A}/+') and homozygote ('*bub-1*^{T527A}') oocytes, as
529 indicated by the yellow lines. Background signal was subtracted and maximum signal
530 for each channel was set to 1.
531 C) Fixed oocytes were stained with a BUB-1 specific antibody (green) and *bub-1*^{T527A}
532 heterozygote and homozygote oocytes were compared. DNA is shown in magenta.
533 D) *bub-1*^{T527A} heterozygote ('*bub-1*^{T527A}/+') and homozygote ('*bub-1*^{T527A}') oocytes
534 expressing GFP-tagged tubulin and mCherry-tagged histone were filmed during
535 meiosis I. Two homozygote ('*bub-1*^{T527A}') oocytes are shown to depict the difference
536 in severity of the alignment defect. Scale bar, 2 µm.
537 E) Meiotic defects (as described in the Methods section) were assessed in wild type, *bub-*
538 *1*^{T527A} heterozygote ('*bub-1*^{T527A}/+') and homozygote oocytes. Representative images
539 of the different phenotypes analysed are presented on the right.
540
541 **Figure 4. CENP-C^{HCP-4} is required for chromosomal PLK-1 targeting.**
542
543 A) *In situ* GFP-tagged CENP-C^{HCP-4} was followed through meiosis I in live, dissected
544 oocytes. Scale bar, 2 µm.
545 B) Schematic representation of the *C. elegans* CENP-C^{HCP-4} (top), sequence alignment of
546 the putative STP motif in nematode species (bottom).

547 C) Control (*'wild type'*) and CENP-C^{HCP-4}-depleted ['*hcp-4(RNAi)'*] oocytes expressing
548 sfGFP-tagged PLK-1 (and mCherry-tagged histone) were dissected and recorded
549 throughout meiosis I. Prometaphase/Metphase I is shown (before spindle
550 rotation/shortening). On the right, the blue arrows point to the midbivalent and the
551 yellow arrow points to the kinetochore. Left scale bar, 2 µm. Right scale bar, 1 µm.
552 D) Line profile analysis of PLK-1::GFP during early Metaphase I in *wild type* and *hcp-*
553 *4(RNAi)* oocytes, as indicated by the yellow lines. Background signal was subtracted
554 and maximum signal for each channel was set to 1. The blue arrows point to the
555 midbivalent and the yellow arrow points to the kinetochore
556
557 **Figure 5. CENP-C^{HCP-4} interacts with PLK-1 in vitro and targets PLK-1 to chromosome**
558 **arms in *C. elegans* oocytes through a polo-docking site.**
559
560 A) Kinase assay of recombinant CENP-C$^{HCP-4(1-214)}$ wild type and T163A proteins with
561 Cdk1:Cyclin B. Reactions were analysed by SDS-PAGE followed by ProQ diamond
562 (phosphoprotein) or coomassie (total protein) staining.
563 B) Elution profile and coomassie-stained SDS-PAGE gels of representative fractions
564 from the Superdex 200 10/300 SEC column. Wild type or T163A mutant CENP-C^{HCP-}
565 $^{4(1-214)}$ was phosphorylated by Cdk1:Cyclin B before incubation with an equimolar
566 concentration of MBP-PLK1^{PBD}. Binding was then assessed by SEC.
567 C) FITC-labelled peptides containing the HCP-4 STP motif were incubated with
568 increasing concentrations of MBP:PLK1^{PBD} and binding analysed by fluoresence
569 polarisation. Unphosphorylated versus T163-phosphorylated (T^{ph}) peptides were
570 compared.

571 D) Control (*'wild type'*) and CENP-C^{HCP-4} STP mutant ['*hcp-4^{T163A}*'] oocytes expressing
572 sfGFP-tagged PLK-1 (and mCherry-tagged histone) were dissected and recorded
573 throughout meiosis I. Metphase I is shown. Left scale bar, 2 µm. Right scale bar, 1
574 µm.
575 E) Line profile analysis of PLK-1::GFP during early Metaphase I in *wild type* and *hcp-*
576 *4^{T163A}* oocytes, as indicated by the yellow lines. Background signal was subtracted and
577 maximum signal for each channel was set to 1.
578 F) Fixed oocytes were stained with an HCP-4 specific antibody (green in the merged
579 image). *hcp-4^{T163A}* mutant oocytes were compared to wild type. DNA is shown in
580 magenta in the merged panel.
581 G) Same as in F) but using a BUB-1 specific antibody to compare BUB-1 localisation in
582 wild type and *hcp-4^{T163A}* mutant oocytes.
583
584 **Figure 6. Combined disruption of BUB-1- and CENP-C^{HCP-4}-dependent PLK-1**
585 **recruitment leads to severe meiotic defects.**
586
587 A) Control (*'wild type'*), BUB-1-depleted ['*bub-1(RNAi)'*], and CENP-C^{HCP-4}-depleted
588 ['*hcp-4(RNAi)'*] oocytes expressing sfGFP-tagged PLK-1 (and mCherry-tagged
589 histone) were dissected and recorded throughout meiosis I. Prometaphase/Metphase I
590 is shown (before spindle rotation/shortening). Left scale bar, 2 µm. Right scale bar, 1
591 µm.
592 B) Control (*'wild type'*), BUB-1-depleted ['*bub-1(RNAi)'*], and CENP-C^{HCP-4}-depleted
593 ['*hcp-4(RNAi)'*] oocytes expressing GFP-tagged tubulin (and mCherry-tagged histone)
594 were dissected and recorded throughout meiosis I. Scale bar, 2 µm.

595 C) Meiotic defects (as described in the Methods section) were assessed in wild type, *bub-*
596 *1(RNAi)*, and *hcp-4(RNAi)* oocytes.
597 D) Fixed wild type, *hcp-4(RNAi)*, *bub-1*^{T527A}, and *bub-1*^{T527A}*+hcp-4(RNAi)* oocytes were
598 stained with a PLK-1 specific antibody.
599 E) Control (*'wild type'*), BUB-1^{T527A} ['*bub-1*^{T527A}*'*], and CENP-C^{HCP-4}-depleted ['*hcp-*
600 *4(RNAi)'*] oocytes expressing GFP-tagged tubulin (and mCherry-tagged histone) were
601 dissected and recorded throughout meiosis I. Scale bar, 2 µm.
602 F) Meiotic defects (as described in the Methods section) were assessed in wild type, *bub-*
603 *1*^{T527A}, *hcp-4(RNAi),* and *bub-1*^{T527A}*+hcp-4(RNAi)* oocytes.
604
605 **Figure S1. PLK-1 localisation during oocyte meiosis**
606 *In situ* GFP-tagged PLK-1 (Martino et al., 2017) was followed through meiosis I in
607 live, dissected oocytes. Scale bar, 2 µm. This panel shows a more detailed sequence of
608 events of the same movie presented in Figure 1B.
609
610 **Figure S2. Embryonic viability assays after PLK-1as inhibition**
611 Three different PP1 analogues were tested: 3IB-PP1, 3MB-PP1, and 1NA-PP1.
612 Inhibitors were included in the plates at 10, 20, and 50 µM and worms were then
613 allowed to lay eggs. Viable progeny was assessed 24 and 48 hs later.
614
615 **Figure S3. Chromosome alignment defects upon acute PLK-1as inhibition**
616
617 A) *Wild type* or *plk-1*^{as} worms expressing GFP-tagged tubulin and mCherry-tagged
618 histone, were dissected in medium containing ethanol, 1 µM 3IB-PP1 ('low'), or 10

619 μM ('high'). Maximum intensity projections are shown and the arrows have different
620 colours to identify those chromosomes in panel B). Scale bar, 2 μm.
621 B) Detailed analysis of individual chromosome behaviour using selected Z slices of
622 +3IB-PP1 'low' from panel A). Highly unstable behaviour of specific chromosomes
623 (switching back and forth between aligned and misaligned) can be followed by the
624 different coloured arrows. Panles outside of the green rectangle are timepoints not
625 shown in A). Scale bar, 2 μm.
626
627 **Figure S4.**
628
629 A) Kinase assay of recominant BUB-1$^{190-628}$ and BUB-1$^{190-628}$(T527A) with Cdk1:Cyclin
630 B. Proteins were incubated with Cdk1:Cyclin B for the indicated time points before
631 phosphorylation was assessed by SDS-PAGE and staining with either coomassie (total
632 protein) or ProQ diamond (phosphoprotein).
633 B) Kinase assay of recominant BUB-1$^{190-628}$ and BUB-1$^{190-628}$(T527A) with PLK-1.
634 Proteins were incubated with PLK-1 for the indicated time points before
635 phosphorylation was assessed by SDS-PAGE and staining with either coomassie (total
636 protein) or ProQ diamond (phosphoprotein).
637
638 **Figure S5.**
639
640 Elution profile and coomassie-stained SDS-PAGE gels of representative fractions
641 from the Superdex 200 10/300 SEC column. CENCP-C$^{HCP-4(1-214)}$ was incubated with
642 MBP-PLK-1^{PBD} at equimolar concentrations before being analysed by SEC. Binding

643 was conducted with unphosphorylated or Cdk1:Cyclin B phosphorylated CENP-C$^{HCP-4(1-214)}$ as indicated.

645

646 **Figure S6.**

647

648 A) Control (*'wild type'*), BUB-1-depleted ['*bub-1(RNAi)'*], CENP-C^{HCP-4}(T163A) ['*hcp-*
649 *4^{T163A}'*], and *bub-1(RNAi)+hcp-4^{T163A}* oocytes expressing sfGFP-tagged PLK-1 (and
650 mCherry-tagged histone) were dissected and recorded throughout meiosis I.
651 Prometaphase/Metphase I is shown (before spindle rotation/shortening). Panels on the
652 left show the full spindle, while the right-most two columns display single bivalents.
653 Left scale bar, 2 µm. Right scale bar, 1 µm.
654 B) Control (*'wild type'*), BUB-1-depleted ['*bub-1(RNAi)'*], CENP-C^{HCP-4}(T163A) ['*hcp-*
655 *4^{T163A}'*], and *bub-1(RNAi)+hcp-4^{T163A}* oocytes expressing GFP-tagged tubulin (and
656 mCherry-tagged histone) were dissected and recorded throughout meiosis I. Scale bar,
657 2 µm.
658 C) Meiotic defects (as described in the Methods section) were assessed in wild type, *bub-*
659 *1(RNAi)*, *hcp-4^{T163A}, and bub-1(RNAi)+hcp-4^{T163A}* oocytes.

660

661

662 **REFERENCES**

663 Archambault V, Glover DM. 2009. Polo-like kinases: conservation and divergence in their
664 functions and regulation. *Nat Rev Mol Cell Biol* **10**:265–275. doi:10.1038/nrm2653
665 Arribere JA, Bell RT, Fu BXH, Artiles KL, Hartman PS, Fire AZ. 2014. Efficient Marker-
666 Free Recovery of Custom Genetic Modifications with CRISPR/Cas9 in
667 Caenorhabditis elegans. *Genetics* **198**:837–846. doi:10.1534/genetics.114.169730
668 Bel Borja L, Soubigou F, Taylor SJP, Fraguas Bringas C, Budrewicz J, Lara-Gonzalez P,
669 Sorensen Turpin CG, Bembenek JN, Cheerambathur DK, Pelisch F. 2020. BUB-1
670 targets PP2A:B56 to regulate chromosome congression during meiosis I in C. elegans
671 oocytes. *eLife* **9**:e65307. doi:10.7554/eLife.65307
672 Bishop AC, Ubersax JA, Petsch DT, Matheos DP, Gray NS, Blethrow J, Shimizu E, Tsien JZ,
673 Schultz PG, Rose MD, Wood JL, Morgan DO, Shokat KM. 2000. A chemical switch
674 for inhibitor-sensitive alleles of any protein kinase. *Nature* **407**:395–401.
675 doi:10.1038/35030148
676 Budirahardja Y, Gönczy P. 2008. PLK-1 asymmetry contributes to asynchronous cell division
677 of *C. elegans* embryos. *Development* **135**:1303–1313. doi:10.1242/dev.019075
678 Cabral G, Laos T, Dumont J, Dammermann A. 2019. Differential Requirements for
679 Centrioles in Mitotic Centrosome Growth and Maintenance. *Developmental Cell*
680 **50**:355-366.e6. doi:10.1016/j.devcel.2019.06.004
681 Chase D, Serafinas C, Ashcroft N, Kosinski M, Longo D, Ferris DK, Golden A. 2000. The
682 polo-like kinase PLK-1 is required for nuclear envelope breakdown and the
683 completion of meiosis inCaenorhabditis elegans. *genesis* **26**:26–41.
684 doi:10.1002/(SICI)1526-968X(200001)26:1<26::AID-GENE6>3.0.CO;2-O
685 Cheerambathur DK, Prevo B, Chow T-L, Hattersley N, Wang S, Zhao Z, Kim T, Gerson-
686 Gurwitz A, Oegema K, Green R, Desai A. 2019. The Kinetochore-Microtubule

Coupling Machinery Is Repurposed in Sensory Nervous System Morphogenesis. *Developmental Cell* **48**:864-872.e7. doi:10.1016/j.devcel.2019.02.002

Cheng K-Y. 2003. The crystal structure of the human polo-like kinase-1 polo box domain and its phospho-peptide complex. *The EMBO Journal* **22**:5757–5768. doi:10.1093/emboj/cdg558

Connolly AA, Sugioka K, Chuang C-H, Lowry JB, Bowerman B. 2015. KLP-7 acts through the Ndc80 complex to limit pole number in C. elegans oocyte meiotic spindle assembly. *Journal of Cell Biology* **210**:917–932. doi:10.1083/jcb.201412010

Conway W, Kiewisz R, Fabig G, Kelleher CP, Wu H-Y, Anjur-Dietrich M, Müller-Reichert T, Needleman DJ. 2022. Self-organization of kinetochore-fibers in human mitotic spindles. *eLife* **11**:e75458. doi:10.7554/eLife.75458

Cordeiro MH, Smith RJ, Saurin AT. 2020. Kinetochore phosphatases suppress autonomous Polo-like kinase 1 activity to control the mitotic checkpoint. *Journal of Cell Biology* **219**:e202002020. doi:10.1083/jcb.202002020

Danlasky BM, Panzica MT, McNally KP, Vargas E, Bailey C, Li W, Gong T, Fishman ES, Jiang X, McNally FJ. 2020. Evidence for anaphase pulling forces during C. elegans meiosis. *Journal of Cell Biology* **219**:e202005179. doi:10.1083/jcb.202005179

Decker M, Jaensch S, Pozniakovsky A, Zinke A, O'Connell KF, Zachariae W, Myers E, Hyman AA. 2011. Limiting Amounts of Centrosome Material Set Centrosome Size in C. elegans Embryos. *Current Biology* **21**:1259–1267. doi:10.1016/j.cub.2011.06.002

Desai A, Rybina S, Müller-Reichert T, Shevchenko Andrej, Shevchenko Anna, Hyman A, Oegema K. 2003. KNL-1 directs assembly of the microtubule-binding interface of the kinetochore in *C. elegans*. *Genes Dev* **17**:2421–2435. doi:10.1101/gad.1126303

710 Dumont J, Oegema K, Desai A. 2010. A kinetochore-independent mechanism drives
711 anaphase chromosome separation during acentrosomal meiosis. *Nat Cell Biol* **12**:894–
712 901. doi:10.1038/ncb2093
713 Elia AEH, Cantley LC, Yaffe MB. 2003a. Proteomic Screen Finds pSer/pThr-Binding
714 Domain Localizing Plk1 to Mitotic Substrates. *Science* **299**:1228–1231.
715 doi:10.1126/science.1079079
716 Elia AEH, Rellos P, Haire LF, Chao JW, Ivins FJ, Hoepker K, Mohammad D, Cantley LC,
717 Smerdon SJ, Yaffe MB. 2003b. The Molecular Basis for Phosphodependent Substrate
718 Targeting and Regulation of Plks by the Polo-Box Domain. *Cell* **115**:83–95.
719 doi:10.1016/S0092-8674(03)00725-6
720 Elowe S, Hümmer S, Uldschmid A, Li X, Nigg EA. 2007. Tension-sensitive Plk1
721 phosphorylation on BubR1 regulates the stability of kinetochore–microtubule
722 interactions. *Genes Dev* **21**:2205–2219. doi:10.1101/gad.436007
723 Foltz DR, Jansen LET, Black BE, Bailey AO, Yates JR, Cleveland DW. 2006. The human
724 CENP-A centromeric nucleosome-associated complex. *Nat Cell Biol* **8**:458–469.
725 doi:10.1038/ncb1397
726 Gelens L, Qian J, Bollen M, Saurin AT. 2018. The Importance of Kinase–Phosphatase
727 Integration: Lessons from Mitosis. *Trends in Cell Biology* **28**:6–21.
728 doi:10.1016/j.tcb.2017.09.005
729 Gigant E, Stefanutti M, Laband K, Gluszek-Kustusz A, Edwards F, Lacroix B, Maton G,
730 Canman JC, Welburn JPI, Dumont J. 2017. Inhibition of ectopic microtubule
731 assembly by the kinesin-13 KLP-7 prevents chromosome segregation and cytokinesis
732 defects in oocytes. *Journal of Cell Science* **130**:e1.1-e1.1. doi:10.1242/jcs.205914
733 Gómez-Cavazos JS, Lee K-Y, Lara-González P, Li Y, Desai A, Shiau AK, Oegema K. 2020.
734 A Non-canonical BRCT-Phosphopeptide Recognition Mechanism Underlies RhoA

Activation in Cytokinesis. *Current Biology* **30**:3101-3115.e11. doi:10.1016/j.cub.2020.05.090

Green RA, Mayers JR, Wang S, Lewellyn L, Desai A, Audhya A, Oegema K. 2013. The midbody ring scaffolds the abscission machinery in the absence of midbody microtubules. *Journal of Cell Biology* **203**:505–520. doi:10.1083/jcb.201306036

Han X, Adames K, Sykes EME, Srayko M. 2015. The KLP-7 Residue S546 Is a Putative Aurora Kinase Site Required for Microtubule Regulation at the Centrosome in C. elegans. *PLoS ONE* **10**:e0132593. doi:10.1371/journal.pone.0132593

Hattersley N, Schlientz AJ, Prevo B, Oegema K, Desai A. 2022. MEL-28/ELYS and CENP-C coordinately control outer kinetochore assembly and meiotic chromosome-microtubule interactions. *Current Biology* **32**:2563-2571.e4. doi:10.1016/j.cub.2022.04.046

Heald R, Tournebize R, Blank T, Sandaltzopoulos R, Becker P, Hyman A, Karsenti E. 1996. Self-organization of microtubules into bipolar spindles around artificial chromosomes in Xenopus egg extracts. *Nature* **382**:420–425. doi:10.1038/382420a0

Heun P, Erhardt S, Blower MD, Weiss S, Skora AD, Karpen GH. 2006. Mislocalization of the Drosophila Centromere-Specific Histone CID Promotes Formation of Functional Ectopic Kinetochores. *Developmental Cell* **10**:303–315. doi:10.1016/j.devcel.2006.01.014

Izuta H, Ikeno M, Suzuki N, Tomonaga T, Nozaki N, Obuse C, Kisu Y, Goshima N, Nomura F, Nomura N, Yoda K. 2006. Comprehensive analysis of the ICEN (Interphase Centromere Complex) components enriched in the CENP-A chromatin of human cells. *Genes to Cells* **11**:673–684. doi:10.1111/j.1365-2443.2006.00969.x

758 Jang C-Y, Coppinger JA, Seki A, Yates JR III, Fang G. 2009. Plk1 and Aurora A regulate the
759 depolymerase activity and the cellular localization of Kif2a. *Journal of Cell Science*
760 **122**:1334–1341. doi:10.1242/jcs.044321
761 Kang YH, Park CH, Kim T-S, Soung N-K, Bang JK, Kim BY, Park J-E, Lee KS. 2011.
762 Mammalian Polo-like Kinase 1-dependent Regulation of the PBIP1-CENP-Q
763 Complex at Kinetochores. *Journal of Biological Chemistry* **286**:19744–19757.
764 doi:10.1074/jbc.M111.224105
765 Kang YH, Park J-E, Yu L-R, Soung N-K, Yun S-M, Bang JK, Seong Y-S, Yu H, Garfield S,
766 Veenstra TD, Lee KS. 2006. Self-Regulated Plk1 Recruitment to Kinetochores by the
767 Plk1-PBIP1 Interaction Is Critical for Proper Chromosome Segregation. *Molecular*
768 *Cell* **24**:409–422. doi:10.1016/j.molcel.2006.10.016
769 Kiewisz R, Fabig G, Conway W, Baum D, Needleman D, Müller-Reichert T. 2022. Three-
770 dimensional structure of kinetochore-fibers in human mitotic spindles. *eLife*
771 **11**:e75459. doi:10.7554/eLife.75459
772 Kitada K, Johnson AL, Johnston LH, Sugino A. 1993. A multicopy suppressor gene of the
773 Saccharomyces cerevisiae G1 cell cycle mutant gene dbf4 encodes a protein kinase
774 and is identified as CDC5. *Molecular and Cellular Biology* **13**:4445–4457.
775 doi:10.1128/mcb.13.7.4445-4457.1993
776 Laband K, Lacroix B, Edwards F, Canman JC, Dumont J. 2018. Chapter 11 - Live imaging of
777 C. elegans oocytes and early embryos In: Maiato H, Schuh M, editors. Methods in
778 Cell Biology, Mitosis and Meiosis Part B. Academic Press. pp. 217–236.
779 doi:10.1016/bs.mcb.2018.03.025
780 Llamazares S, Moreira A, Tavares A, Girdham C, Spruce BA, Gonzalez C, Karess RE,
781 Glover DM, Sunkel CE. 1991. polo encodes a protein kinase homolog required for
782 mitosis in Drosophila. *Genes Dev* **5**:2153–2165. doi:10.1101/gad.5.12a.2153

783 Maddox PS, Corbett KD, Desai A. 2012. Structure, assembly and reading of centromeric
784 chromatin. *Current Opinion in Genetics & Development*, Genome architecture and
785 expression **22**:139–147. doi:10.1016/j.gde.2011.11.005
786 Marston AL, Amon A. 2004. Meiosis: cell-cycle controls shuffle and deal. *Nat Rev Mol Cell*
787 *Biol* **5**:983–997. doi:10.1038/nrm1526
788 Marston AL, Wassmann K. 2017. Multiple Duties for Spindle Assembly Checkpoint Kinases
789 in Meiosis. *Frontiers in Cell and Developmental Biology* **5**.
790 Martino L, Morchoisne-Bolhy S, Cheerambathur DK, Van Hove L, Dumont J, Joly N, Desai
791 A, Doye V, Pintard L. 2017. Channel Nucleoporins Recruit PLK-1 to Nuclear Pore
792 Complexes to Direct Nuclear Envelope Breakdown in C. elegans. *Developmental Cell*
793 **43**:157-171.e7. doi:10.1016/j.devcel.2017.09.019
794 Monen J, Maddox PS, Hyndman F, Oegema K, Desai A. 2005. Differential role of CENP-A
795 in the segregation of holocentric C. elegans chromosomes during meiosis and mitosis.
796 *Nat Cell Biol* **7**:1248–1255. doi:10.1038/ncb1331
797 Mundt KE, Golsteyn RM, Lane HA, Nigg EA. 1997. On the Regulation and Function of
798 Human Polo-like Kinase 1 (PLK1): Effects of Overexpression on Cell Cycle
799 Progression. *Biochemical and Biophysical Research Communications* **239**:377–385.
800 doi:10.1006/bbrc.1997.7378
801 Musacchio A, Desai A. 2017. A Molecular View of Kinetochore Assembly and Function.
802 *Biology* **6**. doi:10.3390/biology6010005
803 Neef R, Preisinger C, Sutcliffe J, Kopajtich R, Nigg EA, Mayer TU, Barr FA. 2003.
804 Phosphorylation of mitotic kinesin-like protein 2 by polo-like kinase 1 is required for
805 cytokinesis. *Journal of Cell Biology* **162**:863–876. doi:10.1083/jcb.200306009
806 Novak B, Kapuy O, Domingo-Sananes MR, Tyson JJ. 2010. Regulated protein kinases and
807 phosphatases in cell cycle decisions. *Current Opinion in Cell Biology*, Cell

808 differentiation / Cell division, growth and death **22**:801–808.
809 doi:10.1016/j.ceb.2010.07.001
810 Oegema K, Desai A, Rybina S, Kirkham M, Hyman AA. 2001. Functional Analysis of
811 Kinetochore Assembly in Caenorhabditis elegans. *Journal of Cell Biology* **153**:1209–
812 1226. doi:10.1083/jcb.153.6.1209
813 Ohkura H. 2015. Meiosis: An Overview of Key Differences from Mitosis. *Cold Spring Harb*
814 *Perspect Biol* **7**:a015859. doi:10.1101/cshperspect.a015859
815 Ohkura H, Hagan IM, Glover DM. 1995. The conserved Schizosaccharomyces pombe kinase
816 plo1, required to form a bipolar spindle, the actin ring, and septum, can drive septum
817 formation in G1 and G2 cells. *Genes Dev* **9**:1059–1073. doi:10.1101/gad.9.9.1059
818 Ohta M, Zhao Z, Wu D, Wang S, Harrison JL, Gómez-Cavazos JS, Desai A, Oegema KF.
819 2021. Polo-like kinase 1 independently controls microtubule-nucleating capacity and
820 size of the centrosome. *Journal of Cell Biology* **220**:e202009083.
821 doi:10.1083/jcb.202009083
822 Okada M, Cheeseman IM, Hori T, Okawa K, McLeod IX, Yates JR, Desai A, Fukagawa T.
823 2006. The CENP-H–I complex is required for the efficient incorporation of newly
824 synthesized CENP-A into centromeres. *Nat Cell Biol* **8**:446–457.
825 doi:10.1038/ncb1396
826 Pahlavan G, Polanski Z, Kalab P, Golsteyn R, Nigg EA, Maro B. 2000. Characterization of
827 Polo-like Kinase 1 during Meiotic Maturation of the Mouse Oocyte. *Developmental*
828 *Biology* **220**:392–400. doi:10.1006/dbio.2000.9656
829 Paix A, Folkmann A, Rasoloson D, Seydoux G. 2015. High Efficiency, Homology-Directed
830 Genome Editing in Caenorhabditis elegans Using CRISPR-Cas9 Ribonucleoprotein
831 Complexes. *Genetics* **201**:47–54. doi:10.1534/genetics.115.179382

832 Paix A, Folkmann A, Seydoux G. 2017. Precision genome editing using CRISPR-Cas9 and
833 linear repair templates in C. elegans. *Methods*, CRISPR-Cas systems for Genome
834 engineering and investigation **121–122**:86–93. doi:10.1016/j.ymeth.2017.03.023
835 Pelisch F, Bel Borja L, Jaffray EG, Hay RT. 2019. Sumoylation regulates protein dynamics
836 during meiotic chromosome segregation in *C. elegans* oocytes. *Journal of Cell*
837 *Science* jcs.232330. doi:10.1242/jcs.232330
838 Pelisch F, Tammsalu T, Wang B, Jaffray EG, Gartner A, Hay RT. 2017. A SUMO-Dependent
839 Protein Network Regulates Chromosome Congression during Oocyte Meiosis.
840 *Molecular Cell* **65**:66–77. doi:10.1016/j.molcel.2016.11.001
841 Petronczki M, Lénárt P, Peters J-M. 2008. Polo on the Rise—from Mitotic Entry to
842 Cytokinesis with Plk1. *Developmental Cell* **14**:646–659.
843 doi:10.1016/j.devcel.2008.04.014
844 Qi W, Tang Z, Yu H. 2006. Phosphorylation- and Polo-Box–dependent Binding of Plk1 to
845 Bub1 Is Required for the Kinetochore Localization of Plk1. *MBoC* **17**:3705–3716.
846 doi:10.1091/mbc.e06-03-0240
847 Rahman MM, Munzig M, Kaneshiro K, Lee B, Strome S, Müller-Reichert T, Cohen-Fix O.
848 2015. Caenorhabditis elegans polo-like kinase PLK-1 is required for merging parental
849 genomes into a single nucleus. *Mol Biol Cell* **26**:4718–4735. doi:10.1091/mbc.E15-
850 04-0244
851 Ritter A, Sanhaji M, Steinhäuser K, Roth S, Louwen F, Yuan J. 2014. The activity regulation
852 of the mitotic centromere-associated kinesin by Polo-like kinase 1. *Oncotarget*
853 **6**:6641–6655. doi:10.18632/oncotarget.2843
854 Sanhaji M, Ritter A, Belsham HR, Friel CT, Roth S, Louwen F, Yuan J. 2014. Polo-like
855 kinase 1 regulates the stability of the mitotic centromere-associated kinesin in mitosis.
856 *Oncotarget* **5**:3130–3144. doi:10.18632/oncotarget.1861

857 Saurin AT. 2018. Kinase and Phosphatase Cross-Talk at the Kinetochore. *Front Cell Dev Biol*
858 **6**:62. doi:10.3389/fcell.2018.00062
859 Schmucker S, Sumara I. 2014. Molecular dynamics of PLK1 during mitosis. *Molecular &*
860 *Cellular Oncology* **1**:e954507. doi:10.1080/23723548.2014.954507
861 Shao H, Huang Y, Zhang L, Yuan K, Chu Y, Dou Z, Jin C, Garcia-Barrio M, Liu X, Yao X.
862 2015. Spatiotemporal dynamics of Aurora B-PLK1-MCAK signaling axis orchestrates
863 kinetochore bi-orientation and faithful chromosome segregation. *Sci Rep* **5**:12204.
864 doi:10.1038/srep12204
865 Sievers F, Wilm A, Dineen D, Gibson TJ, Karplus K, Li W, Lopez R, McWilliam H,
866 Remmert M, Söding J, Thompson JD, Higgins DG. 2011. Fast, scalable generation of
867 high-quality protein multiple sequence alignments using Clustal Omega. *Molecular*
868 *Systems Biology* **7**:539. doi:10.1038/msb.2011.75
869 Singh P, Pesenti ME, Maffini S, Carmignani S, Hedtfeld M, Petrovic A, Srinivasamani A,
870 Bange T, Musacchio A. 2021. BUB1 and CENP-U, Primed by CDK1, Are the Main
871 PLK1 Kinetochore Receptors in Mitosis. *Molecular Cell* **81**:67-87.e9.
872 doi:10.1016/j.molcel.2020.10.040
873 Solc P, Kitajima TS, Yoshida S, Brzakova A, Kaido M, Baran V, Mayer A, Samalova P,
874 Motlik J, Ellenberg J. 2015. Multiple requirements of PLK1 during mouse oocyte
875 maturation. *PLoS One* **10**:e0116783. doi:10.1371/journal.pone.0116783
876 Sunkel CE, Glover DM. 1988. polo, a mitotic mutant of Drosophila displaying abnormal
877 spindle poles. *Journal of Cell Science* **89**:25–38. doi:10.1242/jcs.89.1.25
878 Tavernier N, Noatynska A, Panbianco C, Martino L, Van Hove L, Schwager F, Léger T,
879 Gotta M, Pintard L. 2015. Cdk1 phosphorylates SPAT-1/Bora to trigger PLK-1
880 activation and drive mitotic entry in C. elegans embryos. *Journal of Cell Biology*
881 **208**:661–669. doi:10.1083/jcb.201408064

882 Timmons L, Court DL, Fire A. 2001. Ingestion of bacterially expressed dsRNAs can produce
883 specific and potent genetic interference in Caenorhabditis elegans. *Gene* **263**:103–112.
884 doi:10.1016/S0378-1119(00)00579-5
885 Tong C, Fan H-Y, Lian L, Li S-W, Chen D-Y, Schatten H, Sun Q-Y. 2002. Polo-Like Kinase-
886 1 Is a Pivotal Regulator of Microtubule Assembly During Mouse Oocyte Meiotic
887 Maturation, Fertilization, and Early Embryonic Mitosis1. *Biology of Reproduction*
888 **67**:546–554. doi:10.1095/biolreprod67.2.546
889 Velez-Aguilera G, Nkombo Nkoula S, Ossareh-Nazari B, Link J, Paouneskou D, Van Hove
890 L, Joly N, Tavernier N, Verbavatz J-M, Jantsch V, Pintard L. 2020. PLK-1 promotes
891 the merger of the parental genome into a single nucleus by triggering lamina
892 disassembly. *eLife* **9**:e59510. doi:10.7554/eLife.59510
893 Waterhouse AM, Procter JB, Martin DMA, Clamp M, Barton GJ. 2009. Jalview Version 2—a
894 multiple sequence alignment editor and analysis workbench. *Bioinformatics* **25**:1189–
895 1191. doi:10.1093/bioinformatics/btp033
896 Wianny F, Tavares Á, Evans MJ, Glover DM, Zernicka-Goetz M. 1998. Mouse polo-like
897 kinase 1 associates with the acentriolar spindle poles, meiotic chromosomes and
898 spindle midzone during oocyte maturation. *Chromosoma* **107**:430–439.
899 doi:10.1007/s004120050327
900 Woodruff JB, Wueseke O, Viscardi V, Mahamid J, Ochoa SD, Bunkenborg J, Widlund PO,
901 Pozniakovsky A, Zanin E, Bahmanyar S, Zinke A, Hong SH, Decker M, Baumeister
902 W, Andersen JS, Oegema K, Hyman AA. 2015. Regulated assembly of a
903 supramolecular centrosome scaffold in vitro. *Science* **348**:808–812.
904 doi:10.1126/science.aaa3923
905 Xu J, Shen C, Wang T, Quan J. 2013. Structural basis for the inhibition of Polo-like kinase 1.
906 *Nat Struct Mol Biol* **20**:1047–1053. doi:10.1038/nsmb.2623

Zhang L, Shao H, Huang Y, Yan F, Chu Y, Hou H, Zhu M, Fu C, Aikhionbare F, Fang G, Ding X, Yao X. 2011. PLK1 Phosphorylates Mitotic Centromere-associated Kinesin and Promotes Its Depolymerase Activity*. *Journal of Biological Chemistry* **286**:3033–3046. doi:10.1074/jbc.M110.165340

Zitouni S, Nabais C, Jana SC, Guerrero A, Bettencourt-Dias M. 2014. Polo-like kinases: structural variations lead to multiple functions. *Nat Rev Mol Cell Biol* **15**:433–452. doi:10.1038/nrm3819

916 **METHODS**

917 ***C. elegans* strains & RNAi**

918 Strains used in this study were maintained at 20 degrees unless indicated otherwise. For a
919 complete list of strains, please refer to Table S1.
920 For RNAi-mediated depletions, the targeting sequence for *bub-1* was 2353-2935 and for *hcp-*
921 *4*, 967-2128, both from the first ATG codon. For double depletion, both sequences were
922 cloned in the same vector. All sequences were inserted into L4440 using the NEBuilder HiFi
923 DNA Assembly Master Mix (New England Biolabs) and transformed into DH5a bacteria. The
924 purified plasmids were then transformed into HT115(DE3) bacteria (Timmons et al., 2001).
925 RNAi clones were picked and grown overnight at 37°C in LB with 100 µg/ml ampicillin.
926 Saturated cultures were diluted 1:100 and allowed to grow until reaching an OD600 of 0.8–1.
927 Isopropyl-β-d-thiogalactopyranoside (IPTG) was added to a final concentration of 1 mM, and
928 cultures were incubated for 1 h at 37°C. Bacteria were then seeded onto NGM plates made
929 with agarose and 1 mM IPTG and allowed to dry. L4 worms were then plated on RNAi plates
930 and maintained at 20°C.
931

932 **CRISPR/Cas9**

933 We used direct injection of in vitro–assembled Cas9-CRISPR RNA (crRNA) trans-activating
934 crRNA (tracrRNA) ribonucleoprotein complexes (Paix et al., 2017, 2015).
935 For mutation of Threonine 527 to Alanine in *bub-1*, we used the following crRNA (+ strand):
936 CCCCGCACAAGGAGTTCATT and repair template (- strand):
937 acttacTAATTTACTGAAAGTACTGCTGGTTGGAGCAACAAATACTGGAGCTTCCTGT
938 TCGTGAGTGCTTTCCTCCTCTTTATTTCCGAAATATTCATCAATGTTGACtAAATGA
939 ACTCCTTGTGCGGGgGcactaGTGACGAAATTACCACGAGACGGTTTGAAAAAGCCA
940 AACTCGATTTCATCGTCATAAActaaaa

941

942 For mutation of Threonine 163 to Alanine in *hcp-4*, we used the following crRNA (- strand):
943 TGAAATATCAAGCGATCTCA and repair template (+ strand):
944 taataaatctataatttcagAGTGGAAAAGCTGGATTAAGcTGcagtgCaCCCAAGAGCTCGAGTG
945 ATACGTCGATGAGGTCtTTGAGATCGCTTGATATTTCACATGTCGTCAATACCGAT
946 C
947 Each of the mixes was mixed with dpy-10 crRNA/repair template for screening (Arribere et
948 al., 2014).
949

950 **Live imaging of oocytes**

951 A detailed protocol for live imaging of *C. elegans* oocytes was used with minor modifications
952 (Laband et al., 2018). Fertilized oocytes were dissected and mounted in 5 µl of L-15
953 blastomere culture medium (0.5 mg/mL Inulin; 25 mM HEPES, pH 7.5 in 60% Leibowitz L-
954 15 medium and 20% heat-Inactivated FBS) on 24×40 mm #1.5 coverslips. Once dissection
955 was performed and early oocytes identified using a stereomicroscope, a circle of Vaseline was
956 laid around the sample, and a custom-made 24×40 mm plastic holder (with a centred window)
957 was placed on top. The sample was imaged immediately using 488 nm and 561 nm laser
958 lines. Live imaging was done using a CFI Plan Apochromat Lambda 60X/NA 1.4 oil
959 objective mounted on a microscope (Nikon Eclipse Ti) equiped with a Prime 95B 22mm
960 camera (Photometrics), a spinning-disk head (CSU-X1; Yokogawa Electric Corporation).
961 Acquisition parameters were controlled with NIS software (Nikon). For Figures 1B and 2A,
962 the microscope used was an IX81 (Olympus) equiped with an EMCCD Cascade II camera
963 (Photometrics) and a CSU-X1 spinning disk head (Yokogawa). For all live imaging
964 experiments, partial projections are presented. All files were stored, classified, and managed
965 using OMERO (Allan et al., 2012). Figures were prepared using OMERO.figure and

assembled using Adobe Illustrator. Representative movies shown in Supplementary material were assembled using Fiji/ImageJ (Schindelin et al., 2012) custom-made macros.

Immunofluorescence

Worms were placed on 4 µl of M9 worm buffer in a poly-D-lysine (Sigma, P1024)-coated slide and a 24×24-cm coverslip was gently laid on top. Once the worms extruded the embryos, slides were placed on a metal block on dry ice for >10 min. The coverslip was then flicked off with a scalpel blade, and the samples were fixed in methanol at 20°C for 30 min (except for GFP, where the methanol treatment lasted 5 min). Secondary antibodies were donkey anti–sheep, goat anti-mouse, or goat anti-rabbit conjugated to Alexa Fluor™ 488, Alexa Fluor™ 594, and Alexa Fluor™ 647 (1:1,000, Thermo Scientific). Donkey anti-mouse and donkey anti-rabbit conjugated secondary antibodies were obtained from Jackson ImmunoReserach. Embryos were mounted in ProLong Diamond antifade mountant (Thermo Scientific) with DAPI. Primary antibodies were: α-PLK-1 (Budirahardja and Gönczy, 2008), α-HCP-4 (Oegema et al., 2001), α-BUB-1, purified in house after immunisation of rabbits using the sequence in (Desai et al., 2003),

Sequence alignments

Sequences shown in Figures 2C and 4B were aligned with Clustal Omega (Sievers et al., 2011) and visualised with Jalview (Waterhouse et al., 2009).

Protein Purification

GST-BUB-1$^{190-628}$ and GST-HCP-4$^{1-214}$ proteins were expressed in *Escherichia coli* BL21 DE3 bacteria by diluting a saturated culture 1/100 in LB media supplemented with 35 µg/ml ampicillin and incubating at 37°C/200 rpm until OD_{600} 0.6-0.8 was reached. IPTG was then

991 added to a final concentration of 100 µM and cultures were incubated at 20ºC/200 rpm for 16-
992 18 h. The bacterial cultures were then centrifuged (20 min/6,250 g/4ºC) and pellets
993 resuspended in lysis buffer (50 mM Tris-HCl, pH 7.5; 150 mM NaCl; 0.5 mM TCEP, 1X
994 Roche cOmplete protease inhibitors, EDTA free; 30-35 ml/L of culture). The cell suspension
995 was then sonicated (2 min 40 sec, 20 sec on/40 sec off) before centrifugation (45 min, 27,250
996 g, 4ºC) to remove insoluble material. GSH sepharose beads were washed with 10 column
997 volumes (CV) of MilliQ water and equilibrated with 10 CV of binding buffer (50 mM Tris-
998 HCl, pH 7.5, 150 mM NaCl, 0.5 mM TCEP) before filtered (0.22 µm PES filter) lysate was
999 added and batch bound at 4ºC for 1.5-2 h. The beads were then collected in a column and
1000 washed with at least 10 CV of binding buffer before being transferred to a falcon tube and
1001 incubated overnight with GST-tagged 3C protease. After cleavage, the beads were collected
1002 in a column and the flowthrough containing cleaved protein was concentrated in a Vivaspin
1003 centrifugal concentrator. The protein was then further purified by size exclusion
1004 chromatography in a Superdex 200 10/300 column (run in SEC buffer, see below) and
1005 concentrated before being flash frozen in liquid nitrogen and stored at –80.
1006 MBP-PLK1^{PBD} (6xHIS-MBP tagged human PLK1$^{345-603}$, as per (Singh et al., 2021)) was
1007 expressed and purified in the same manner as the GST tagged proteins with the following
1008 exceptions: filtered lysate was passed through a cobalt-NTA column and washed with at least
1009 10 CV of binding buffer (see buffers below) before elution in 0.5 CV fractions. Fractions
1010 containing the protein were concentrated using Vivapsin centrifugal filters and further
1011 purified by size exclusion chromatography (Superdex 200 10/300) in SEC buffer. Lysis buffer
1012 (50 mM Tris-HCl, pH 7.5; 500 mM NaCl; 10 mM imidazole; 0.5 mM TCEP; 1X Roche
1013 cOmplete protease inhibitors, EDTA free; 50 ml/L of culture); binding buffer (50 mM Tris-
1014 HCl, pH 7.5; 500 mM NaCl; 10 mM imidazole; 0.5 mM TCEP); elution buffer (50 mM Tris-

1015 HCl, pH 7.5; 150 mM NaCl; 200 mM imidazole; 0.5 mM TCEP); SEC buffer (50 mM Tris-
1016 HCl, pH 7.5, 150 mM NaCl, 0.5 mM TCEP).
1017
1018 **Kinase assays**
1019 Unless otherwise stated, kinase assays were conducted with 55 nM Cdk1:Cyclin B (Thermo
1020 Scientific) and/or 75 nM PLK-1, produced as described in (Tavernier et al., 2015), at 30ºC in
1021 kinase buffer: 50 mM Tris-HCl, pH 7.5; 1 mM ATP; 10 mM $MgCl_2$; 0.5 mM TCEP; 0.1 mM
1022 EDTA. For the assays in Figure 2E and Figure S4; 0.4 µg/µl (8.2 µM) of BUB-$1^{190-628}$
1023 substrate was used and incubated under the above conditions for up to 2 h. The assay in
1024 Figure 5A was conducted in the above conditions for up to 1 h with a substrate concentration
1025 of 0.2 µg/µl (8.2 µM). The assay in Figure 2D was conducted with 165 nM Cdk1:Cyclin B
1026 and 170 nM PLK-1 and incubated for 30 min at 37ºC with the following buffer: 40 mM Tris-
1027 HCl, pH 7.5; 100 µM ATP, 10 mM $MgCl_2$. BUB-$1^{190-628}$ concentration was 0.2 µg/µl (4.1
1028 µM).
1029 In all assays, aliquots of protein at the indicated timepoints were immediately added to an
1030 equal volume of 2X LDS buffer (Thermo) and incubated at 70 degrees for 15 min. Assays
1031 were assessed by SDS-PAGE combined with ProQ diamond phosphoprotein and coomassie
1032 staining.
1033
1034 ***In vitro* Binding Assays**
1035 BUB-$1^{190-628}$ or CENP-$C^{HCP-4(1-214)}$ recombinant proteins were incubated for 50-60 min at
1036 30ºC in the presence or absence of ~100 nM Cdk1:Cyclin B in kinase buffer (see 'kinase
1037 assay' section of methods). The respective proteins were then incubated for 50 min on ice
1038 with MBP-$PLK1^{PBD}$ at a concentration of 20 µM in SEC buffer (50 mM Tris-HCl, pH 7.5;
1039 150 mM NaCl; 0.5 mM TCEP). Assays were then centrifuged (13.3k rpm, 10 min, 4ºC)

1040 before being loaded onto a Superdex 200 10/300 SEC column. In all assays, 0.2 ml fractions
1041 were collected and selected fractions were assessed by SDS-PAGE with coomassie staining.
1042 More specifically; for the binding assays with BUB-1$^{190-628}$ in Figure 2F-G, 200 µl of binding
1043 assay was loaded into a 0.5 ml loop and loaded onto the column with 2 ml of SEC buffer. For
1044 the CENP-C$^{HCP-4(1-214)}$ assays in Figure 5B and Figure S5, 100 µl of assay was loaded onto
1045 a100 µl loop and loaded onto the column with 0.4 ml of SEC buffer.
1046
1047 **Fluoresence Polarisation**
1048 Fluoresence polarisation assays were conducted using FITC-labelled peptides (peptide
1049 sequences indicated in figures). For all assays: a 1:2 dilution series of MBP-PLK1^{PBD} was
1050 conducted in FP buffer (50 mM Tris-HCl, pH 7.5, 150 mM NaCl, 0.5 mM TCEP) with a
1051 constant concentration of 100 nM FITC-labelled peptide. Assays were left for 10-30 min
1052 before briefly centrifuged and 10 µl of each concentration was loaded onto a black 384 well
1053 plate (Greiner) in triplicate. Plates were then centrifuged (2k rpm, 2 min) before being
1054 analysed in a PheraStar FS (BMG Labtech) under the following conditions: excitation: 485
1055 nm, emission: 520 nm, 25°C, positioning delay 0.3 s, 50 flashes per well, 9.3 mm focal
1056 height. Average mP for each triplicate was then plotted against the MBP-PLK1^{PBD}
1057 concentration using and a non-linear curve fitted using GraphPad Prism 'One Site – Total'
1058 equation.
1059
1060 **Phenotype Analysis**
1061 We defined misalignment as metaphase defects. Alignment was counted within the 5 frames
1062 (1 min) before anaphase onset, which was the frame prior to the detection of two separating
1063 chromosome masses. When one bivalent was misaligned (either in angle or distance to

1064 metaphase plate) it was recorded as mild metaphase defect. When two or more bivalents were
1065 misaligned, this was considered as a severe metaphase defect.
1066 The anaphase phenotype was assess during segregation. If lagging chromosome were detected
1067 during chromosome segregation but this was resolved before polar body extrusion, it was
1068 scored as mild anaphase defect. If we could not detect two segregating masses of
1069 chromosomes or if these masses differed in size/intensity, it was quantified as a severe
1070 anaphase defect.
1071 Polar body defect was recorded when no polar body was extruded or if all of the maternal
1072 DNA content was extruded as a polar body, with no maternal DNA remaining in the
1073 cytoplasm.
1074 Graphs were prepared using Graphpad Prism 9.0.
1075

1076 **Table S1**: *C. elegans* strains used in this study

GFP::tubulin; mCherry::histone	OD868	*ltSi220[pOD1249/pSW077; Pmex-5::GFP::tbb-2::operon_linker::mCHerry::his-11; cb-unc-119(+)]I*	(Green et al., 2013) PMID: 24217623
GFP::HCP-4	OD3410	*hcp-4(lt72[GFP::hcp-4])I*	(Cheerambathur et al., 2019) PMID: 30827898
PLK-1::sfGFP	OD2425	*plk-1(lt18[plk-1::sGFP]::loxp)III*	(Martino et al., 2017) PMID: 29065307
GFP::ASPM-1	EU2861	*or1935[GFP::aspm-1]I*	(Connolly et al., 2015) PMID: 26370499
PLK-1::sfGFP; mCherry::histone	FGP263	*plk-1(lt18[plk-1::sGFP]::loxp)III; ltIs37 [pAA64; pie-1/mCHERRY::his-58; unc-119 (+)]IV*	This study
hcp-4(T163A)	FGP669	*hcp-4(fgp58[hcp-4(T163A)])I*	This study
bub-1(T527A)/hT2	FGP672	*bub-1(fgp4[bub-1(T527A)])I; hT2 [bli-4(e937) let-?(q782) qIs48](I;III)*	This study
plk-1(as)	OD3697	*plk-1((lt106[plk-1 C52V] lt109[plk-1 L115G])III*	(Gómez-Cavazos et al., 2020) PMID: 32619481
GFP::tubulin; mCherry::histone; bub-1(T527A)/hT2	FGP674	*ltSi220[pOD1249/pSW077; Pmex-5::GFP::tbb-2::operon_linker::mCHerry::his-11; cb-unc-119(+)]I; bub-1(fgp4[bub-1(T527A)])I; hT2 [bli-4(e937) let-?(q782) qIs48](I;III)*	This study

GFP::tubulin; mCherry::histone; plk-1(as)	FGP675	*ltSi220[pOD1249/pSW077; Pmex-5::GFP::tbb-2::operon_linker::mCHerry::his-11; cb-unc-119(+)]I; plk-1((lt106[plk-1 C52V] lt109[plk-1 L115G])III*	This study
PLK-1::sGFP; mCherry::histone; hcp-4(T163A)	FGP719	*plk-1(lt18[plk-1::sGFP]::loxp)III; ltIs37 [pAA64; pie-1/mCHERRY::his-58; unc-119 (+)]IV; hcp-4(fgp58[hcp-4(T163A)])I*	This study
GFP::ASPM-1; mCherry::histone; plk-1(as)	FGP725	*or1935[GFP::aspm-1] I; itIs37[pie-1p::mCherry::H2B::pie-1 3'UTR + unc-119(+)] IV; plk-1((lt106[plk-1 C52V] lt109[plk-1 L115G])III*	This study
GFP::HCP-4; mCherry::histone; TIR1	FGP311	*hcp-4(lt72[GFP::hcp-4])I; ltIs37 [pAA64; pie-1/mCHERRY::his-58; unc-119 (+)]IV)I; ieSi65 [sun-1p::TIR1::sun-1 3'UTR + Cbr-unc-119(+)] II; unc-119(ed3)III*	This study

1077

Figure 1

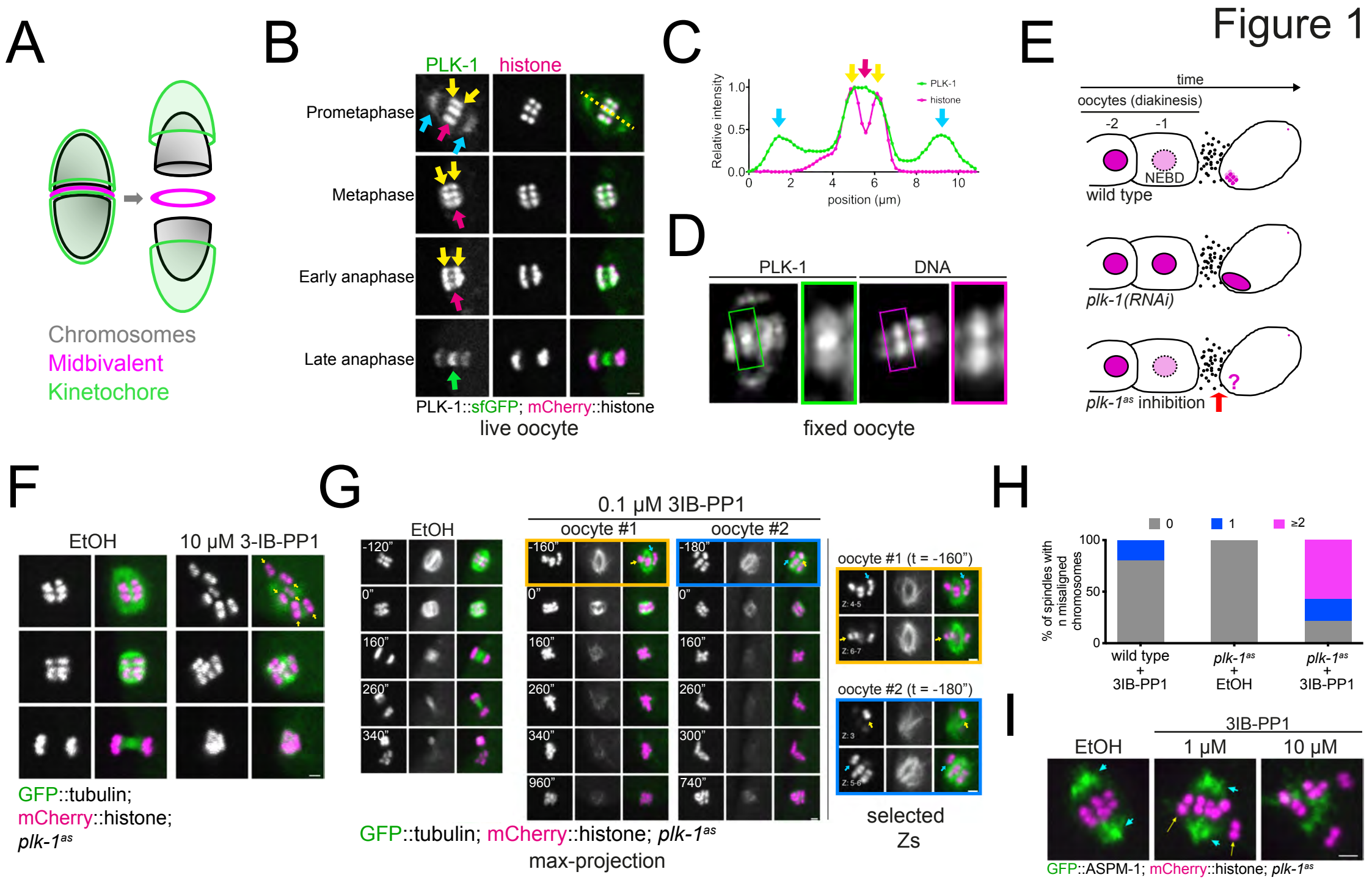
A
Chromosomes
Midbivalent
Kinetochore
B
PLK-1
histone
Prometaphase
Metaphase
Early anaphase
Late anaphase
PLK-1::sfGFP; mCherry::histone
live oocyte
C
Relative intensity
1.0
0.5
0.0
0
2
4
6
8
10
position (µm)
PLK-1
histone
D
PLK-1
DNA
fixed oocyte
E
time
oocytes (diakinesis)
-2
-1
NEBD
wild type
plk-1(RNAi)
plk-1as inhibition
?
F
EtOH
10 µM 3-IB-PP1
GFP::tubulin;
mCherry::histone;
plk-1as
G
0.1 µM 3IB-PP1
EtOH
oocyte #1
oocyte #2
-120"
0"
160"
260"
340"
-160"
0"
160"
260"
340"
960"
-180"
0"
160"
260"
300"
740"
oocyte #1 (t = -160")
oocyte #2 (t = -180")
selected
Zs
GFP::tubulin; mCherry::histone; plk-1as
max-projection
H
0
1
≥2
% of spindles with n misaligned chromosomes
100
50
0
wild type + 3IB-PP1
plk-1as + EtOH
plk-1as + 3IB-PP1
I
3IB-PP1
EtOH
1 µM
10 µM
GFP::ASPM-1; mCherry::histone; plk-1as

Figure 2

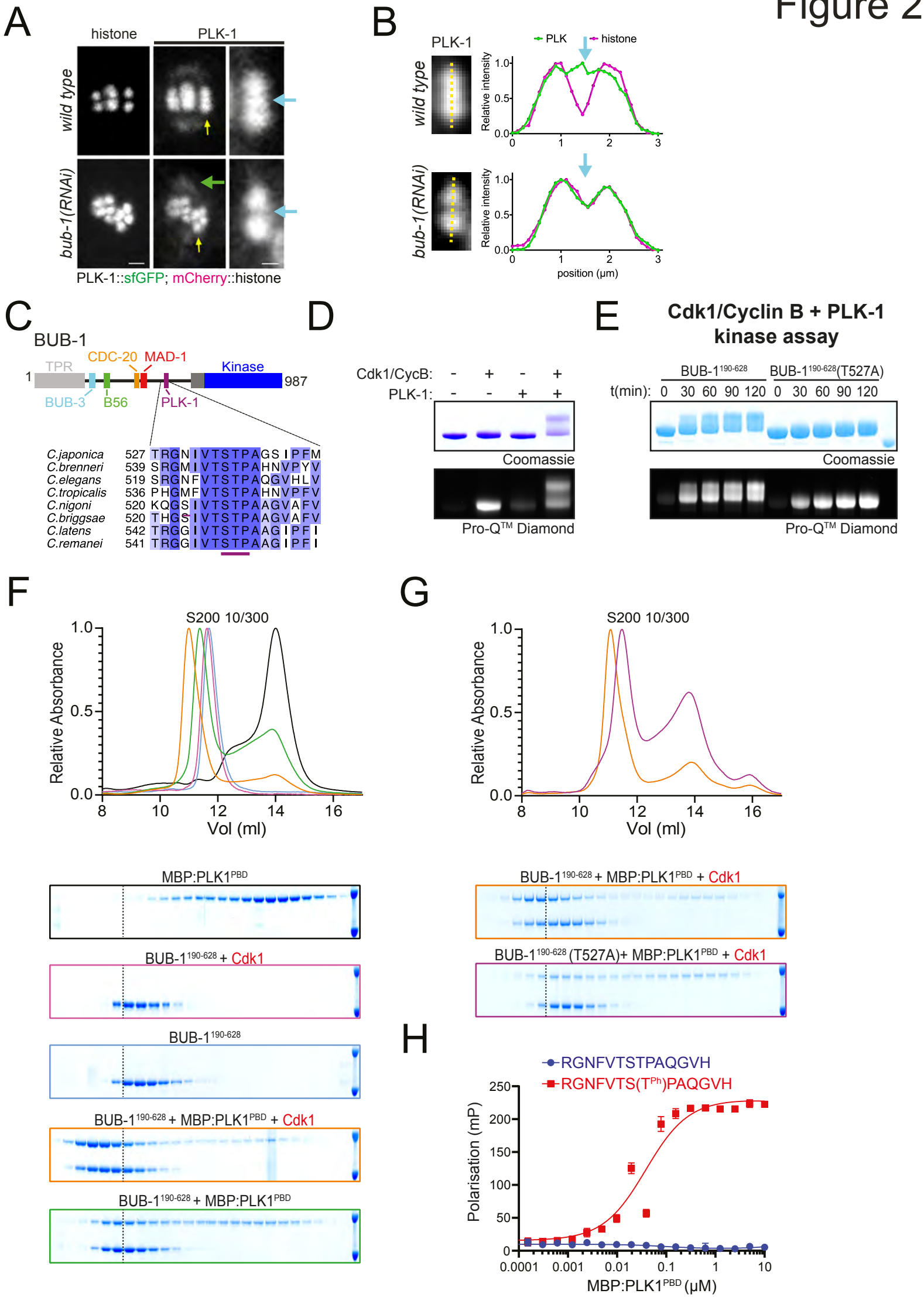
A
histone
PLK-1
wild type
bub-1(RNAi)
PLK-1::sfGFP; mCherry::histone
B
PLK-1
PLK
histone
Relative intensity
position (µm)
C
BUB-1
TPR
CDC-20
MAD-1
Kinase
1
987
BUB-3
B56
PLK-1
C.japonica 527 TRGNIVTSTPAGSIPFM
C.brenneri 539 SRGMIVTSTPAHNVPYV
C.elegans 519 SRGNFVTSTPAQGVHLV
C.tropicalis 536 PHGMFVTSTPAHNVPFV
C.nigoni 520 KQGSIVTSTPAAGVAFV
C.briggsae 520 THGSIVTSTPAAGVAFV
C.latens 542 TRGGIVTSTPAAGIPFI
C.remanei 541 TRGGIVTSTPAAGIPFI
D
Cdk1/CycB:
PLK-1:
Coomassie
Pro-Q™ Diamond
E
Cdk1/Cyclin B + PLK-1 kinase assay
BUB-1190-628
BUB-1190-628(T527A)
t(min): 0 30 60 90 120 0 30 60 90 120
Coomassie
Pro-Q™ Diamond
F
S200 10/300
Relative Absorbance
Vol (ml)
MBP:PLK1PBD
BUB-1190-628 + Cdk1
BUB-1190-628
BUB-1190-628 + MBP:PLK1PBD + Cdk1
BUB-1190-628 + MBP:PLK1PBD
G
S200 10/300
Relative Absorbance
Vol (ml)
BUB-1190-628 + MBP:PLK1PBD + Cdk1
BUB-1190-628 (T527A)+ MBP:PLK1PBD + Cdk1
H
RGNFVTSTPAQGVH
RGNFVTS(TPh)PAQGVH
Polarisation (mP)
MBP:PLK1PBD (µM)

Figure 3

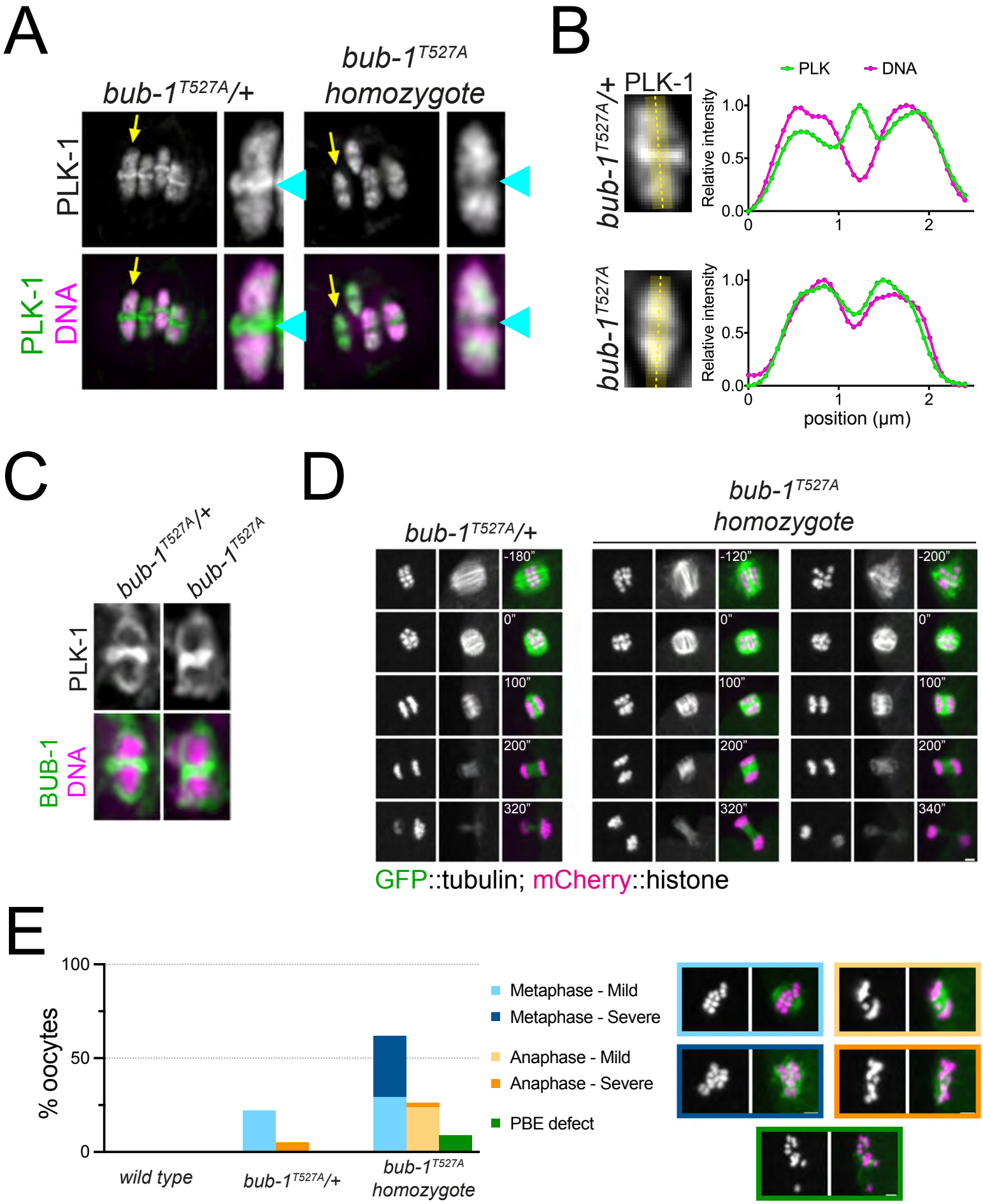
A
bub-1T527A/+
bub-1T527A homozygote
PLK-1
PLK-1
DNA
B
PLK-1
PLK
DNA
bub-1T527A/+
bub-1T527A
Relative intensity
1.0
0.5
0.0
0
1
2
position (μm)
C
bub-1T527A/+
bub-1T527A
PLK-1
BUB-1
DNA
D
bub-1T527A/+
bub-1T527A homozygote
-180"
0"
100"
200"
320"
-120"
-200"
340"
GFP::tubulin; mCherry::histone
E
% oocytes
100
50
0
wild type
bub-1T527A/+
bub-1T527A homozygote
Metaphase - Mild
Metaphase - Severe
Anaphase - Mild
Anaphase - Severe
PBE defect

Figure 4

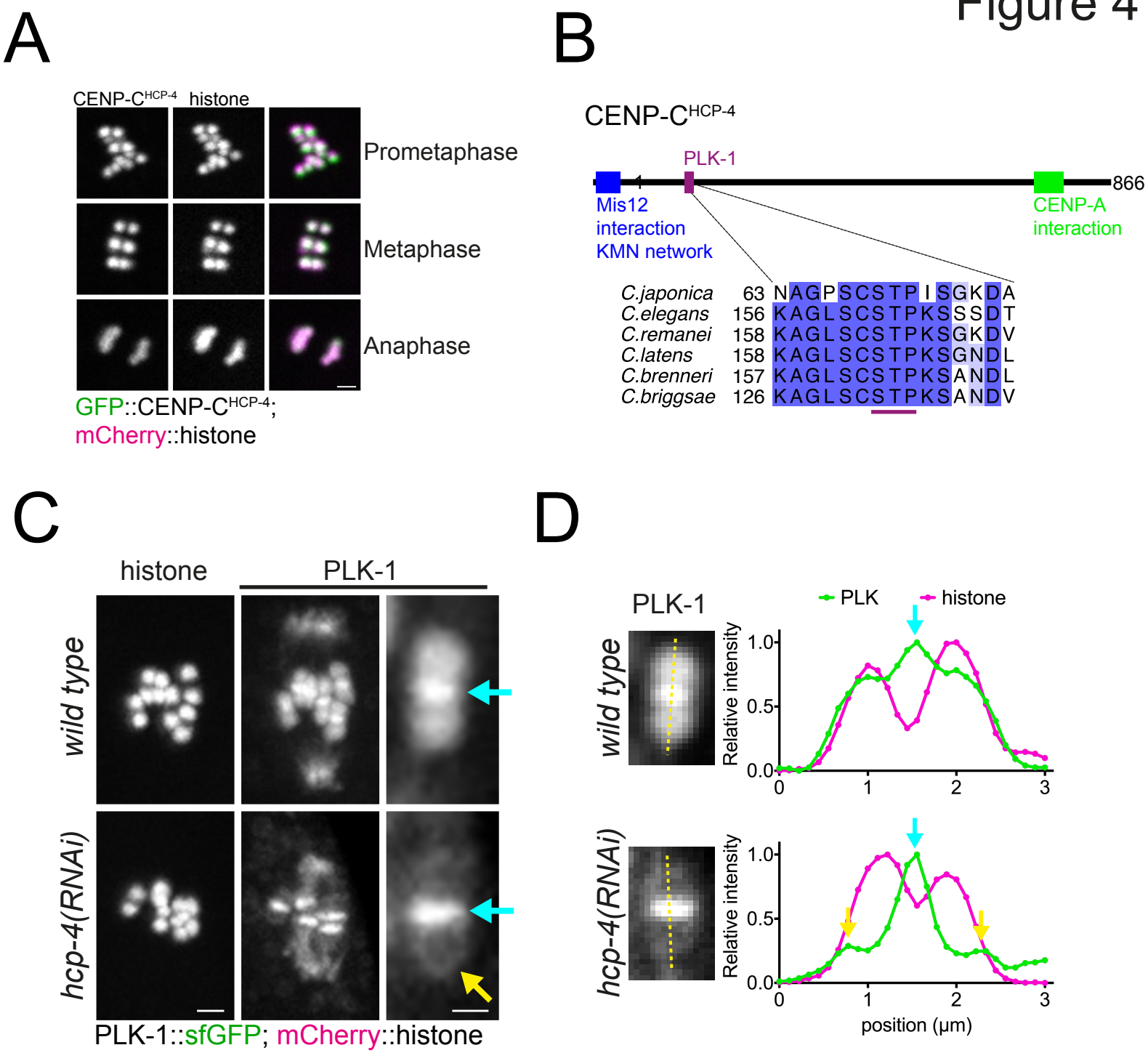
A
CENP-C^HCP-4
histone
Prometaphase
Metaphase
Anaphase
GFP::CENP-C^HCP-4;
mCherry::histone
B
CENP-C^HCP-4
PLK-1
1
866
Mis12
interaction
KMN network
CENP-A
interaction
C.japonica 63 NAGPSCSTPISGKDA
C.elegans 156 KAGLSCSTPKSSSDT
C.remanei 158 KAGLSCSTPKSGKDV
C.latens 158 KAGLSCSTPKSGNDL
C.brenneri 157 KAGLSCSTPKSANDL
C.briggsae 126 KAGLSCSTPKSANDV
C
histone
PLK-1
wild type
hcp-4(RNAi)
PLK-1::sfGFP; mCherry::histone
D
PLK-1
PLK
histone
wild type
hcp-4(RNAi)
Relative intensity
1.0
0.5
0.0
0
1
2
3
position (μm)

Figure 5

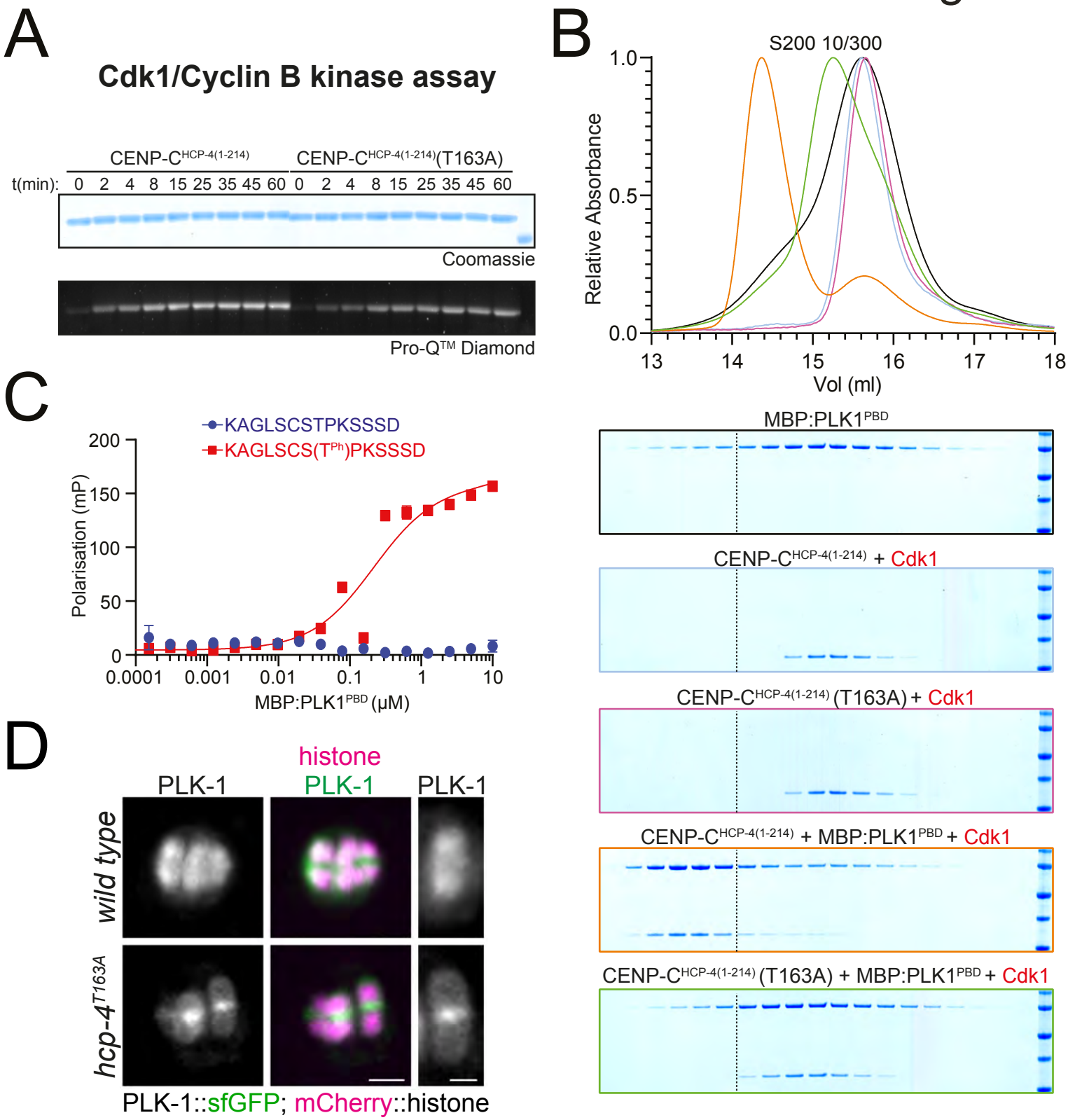
A
Cdk1/Cyclin B kinase assay
CENP-C HCP-4(1-214)
CENP-C HCP-4(1-214)(T163A)
t(min): 0 2 4 8 15 25 35 45 60 0 2 4 8 15 25 35 45 60
Coomassie
Pro-Q™ Diamond
B
S200 10/300
Relative Absorbance
Vol (ml)
C
KAGLSCSTPKSSSD
KAGLSCS(TPh)PKSSSD
Polarisation (mP)
MBP:PLK1PBD (μM)
MBP:PLK1PBD
CENP-C HCP-4(1-214) + Cdk1
CENP-C HCP-4(1-214) (T163A) + Cdk1
CENP-C HCP-4(1-214) + MBP:PLK1PBD + Cdk1
CENP-C HCP-4(1-214) (T163A) + MBP:PLK1PBD + Cdk1
D
histone
PLK-1
PLK-1
PLK-1
wild type
hcp-4T163A
PLK-1::sfGFP; mCherry::histone
E
PLK-1
PLK
DNA
wild type
hcp-4T163A
Relative intensity
position (μm)
F
DNA
HCP-4
HCP-4
DNA
wild type
hcp-4T163A
G
wild type
hcp-4T163A
PLK-1
BUB-1
DNA

Figure 6

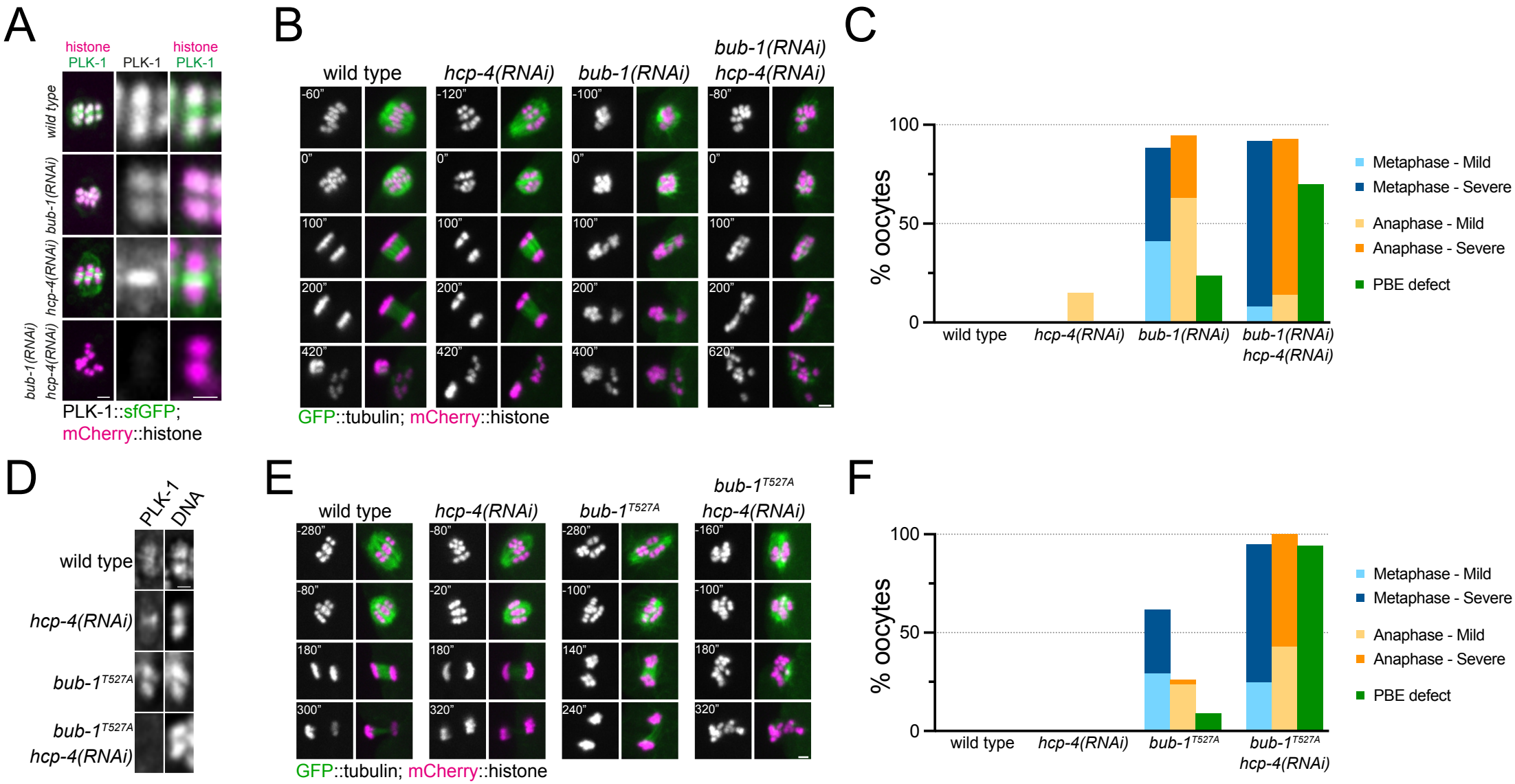
A
histone
PLK-1
PLK-1
histone
PLK-1
wild type
bub-1(RNAi)
hcp-4(RNAi)
bub-1(RNAi)
hcp-4(RNAi)
PLK-1::sfGFP;
mCherry::histone
B
wild type
hcp-4(RNAi)
bub-1(RNAi)
bub-1(RNAi)
hcp-4(RNAi)
-60"
0"
100"
200"
420"
-120"
0"
100"
200"
420"
-100"
0"
100"
200"
400"
-80"
0"
100"
200"
620"
GFP::tubulin; mCherry::histone
C
% oocytes
100
50
0
wild type
hcp-4(RNAi)
bub-1(RNAi)
bub-1(RNAi)
hcp-4(RNAi)
Metaphase - Mild
Metaphase - Severe
Anaphase - Mild
Anaphase - Severe
PBE defect
D
PLK-1
DNA
wild type
hcp-4(RNAi)
bub-1T527A
bub-1T527A
hcp-4(RNAi)
E
wild type
hcp-4(RNAi)
bub-1T527A
bub-1T527A
hcp-4(RNAi)
-280"
-80"
180"
300"
-80"
-20"
180"
320"
-280"
-100"
140"
240"
-160"
-100"
180"
320"
GFP::tubulin; mCherry::histone
F
% oocytes
100
50
0
wild type
hcp-4(RNAi)
bub-1T527A
bub-1T527A
hcp-4(RNAi)
Metaphase - Mild
Metaphase - Severe
Anaphase - Mild
Anaphase - Severe
PBE defect

Figure S1

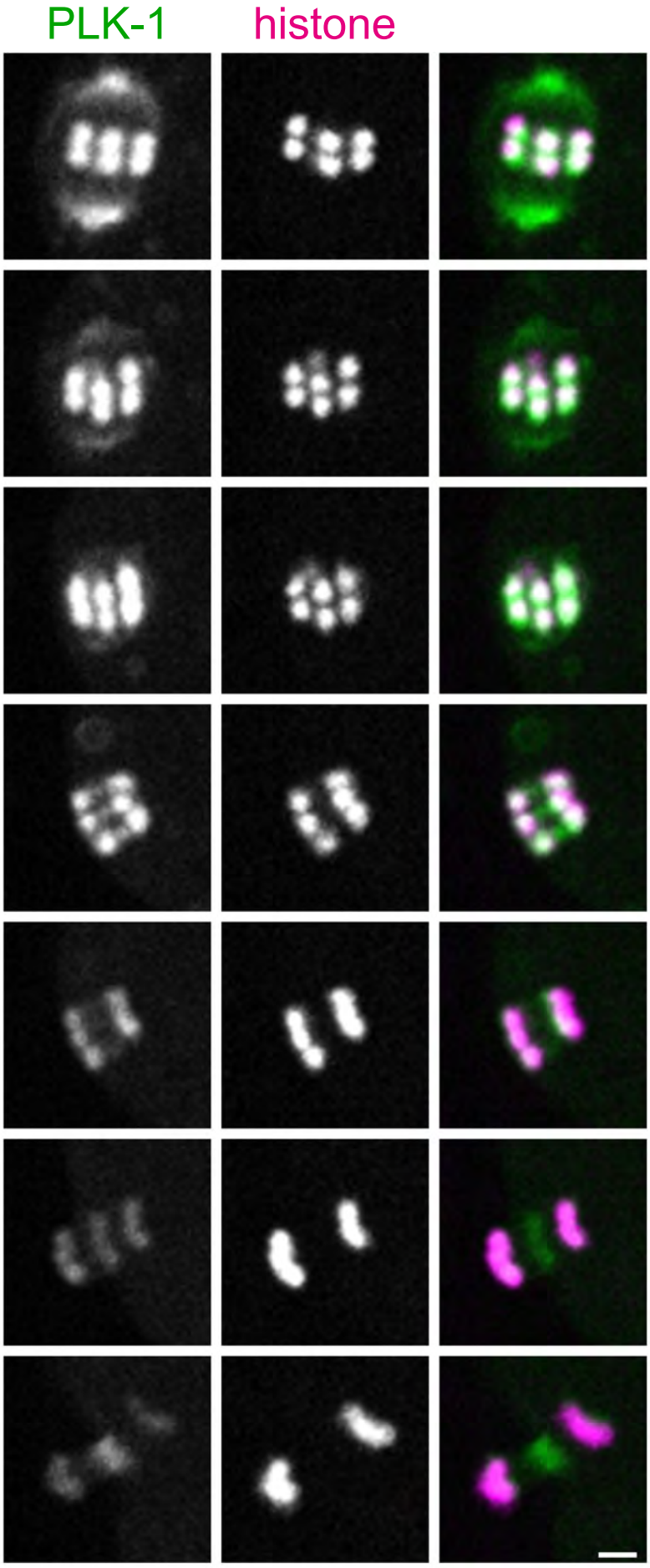

PLK-1::sfGFP; mCherry::histone

Figure S2

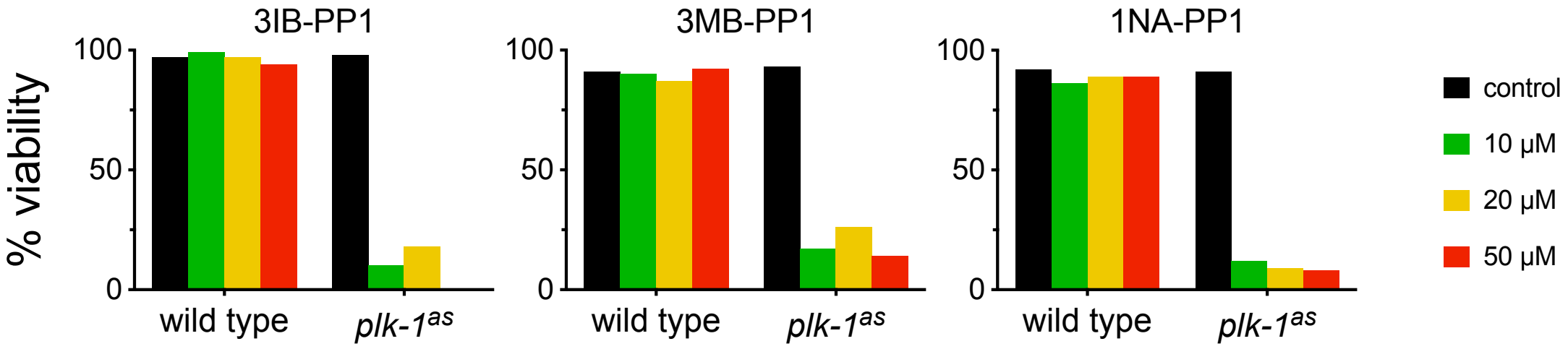
3IB-PP1
3MB-PP1
1NA-PP1
% viability
100
50
0
wild type
plk-1as
control
10 μM
20 μM
50 μM

Figure S3

A

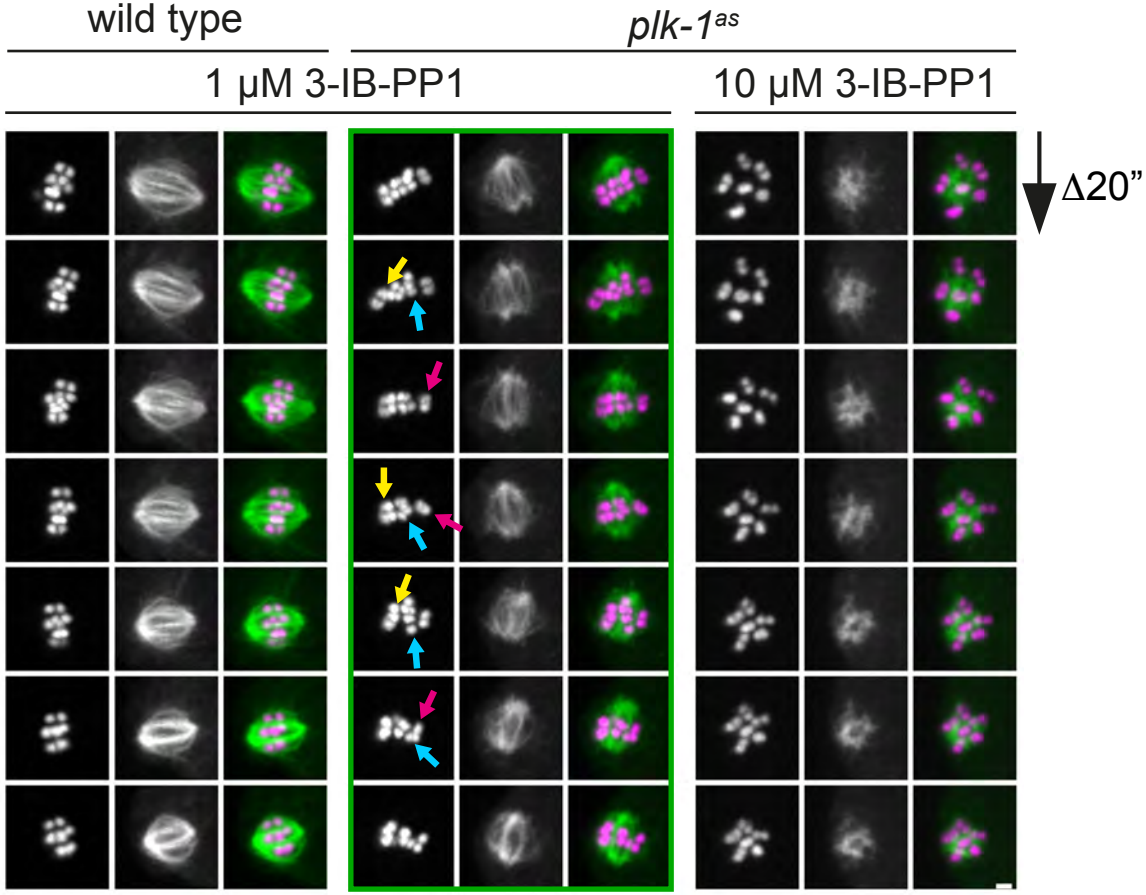

GFP::tubulin; mCherry::histone

B

GFP::tubulin; mCherry::histone

Figure S4

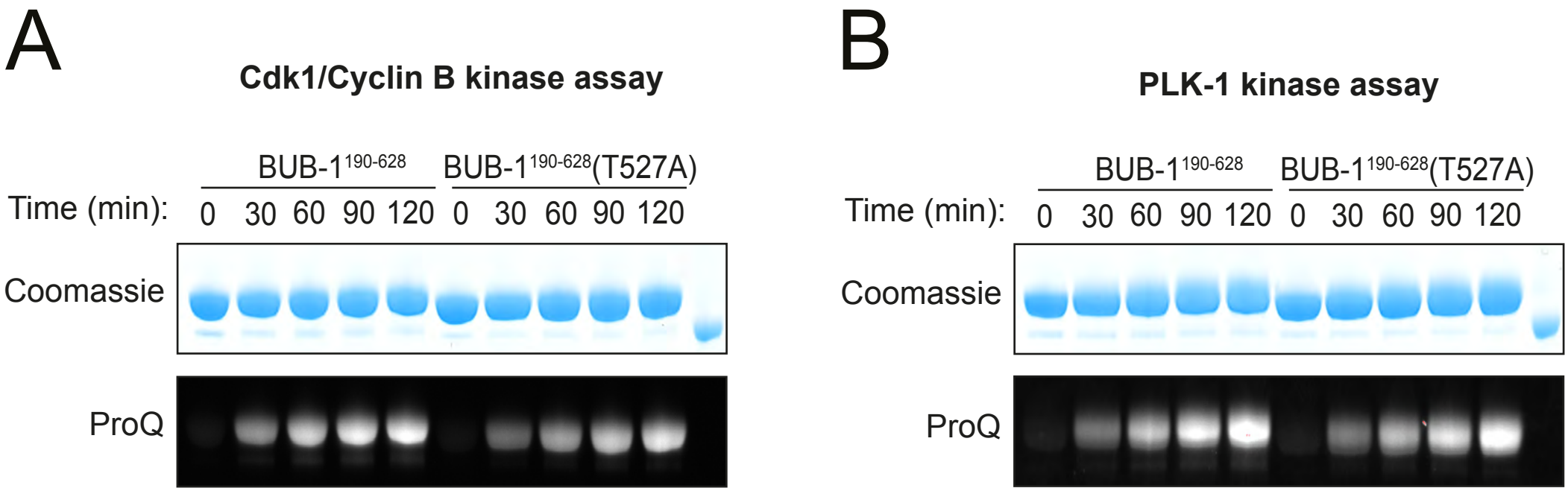
A
Cdk1/Cyclin B kinase assay
BUB-1190-628
BUB-1190-628(T527A)
Time (min):
0 30 60 90 120 0 30 60 90 120
Coomassie
ProQ
B
PLK-1 kinase assay
BUB-1190-628
BUB-1190-628(T527A)
Time (min):
0 30 60 90 120 0 30 60 90 120
Coomassie
ProQ

Figure S5

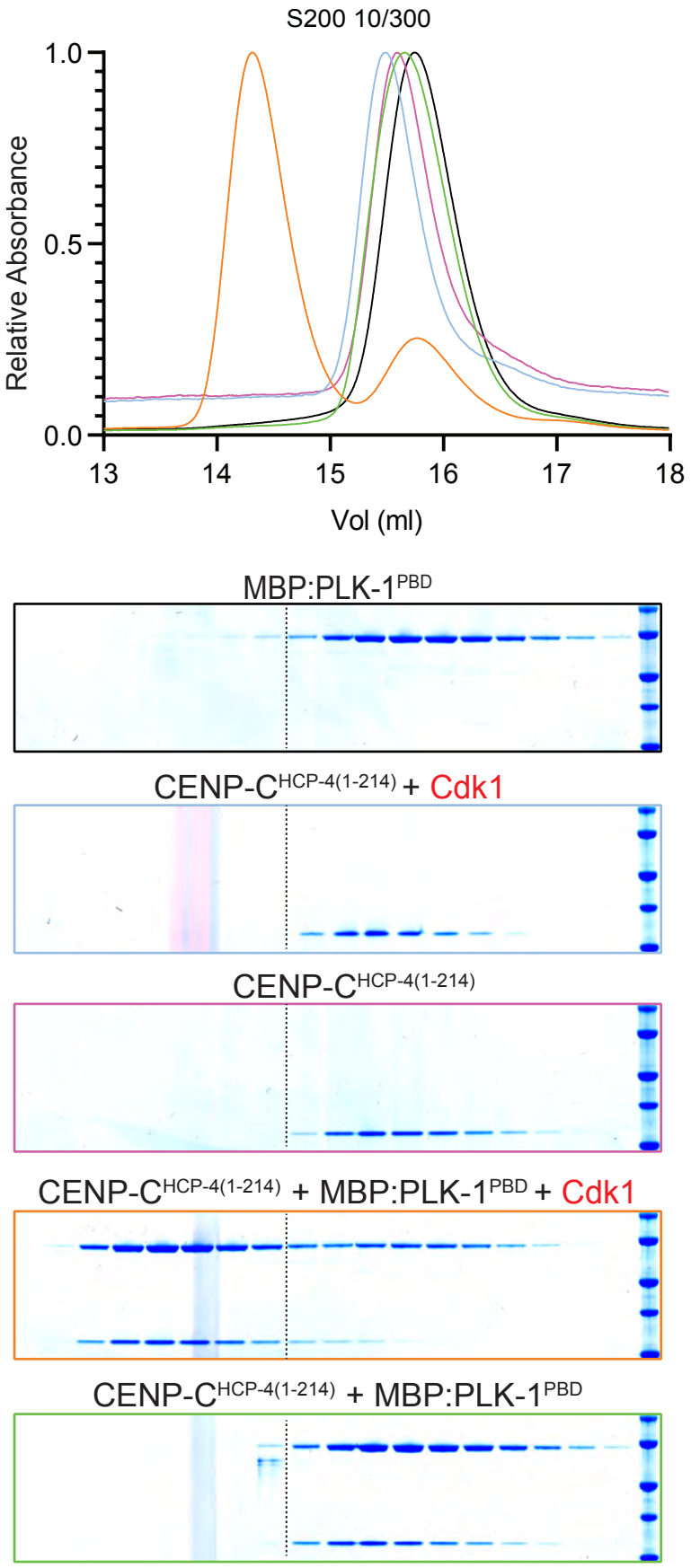
S200 10/300
Relative Absorbance
1.0
0.5
0.0
13
14
15
16
17
18
Vol (ml)
MBP:PLK-1PBD
CENP-CHCP-4(1-214) + Cdk1
CENP-CHCP-4(1-214)
CENP-CHCP-4(1-214) + MBP:PLK-1PBD + Cdk1
CENP-CHCP-4(1-214) + MBP:PLK-1PBD

Figure S6

A

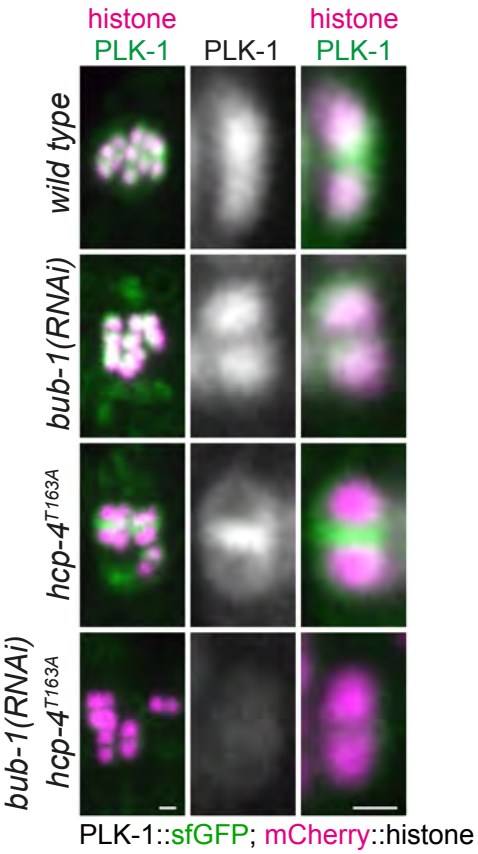

B

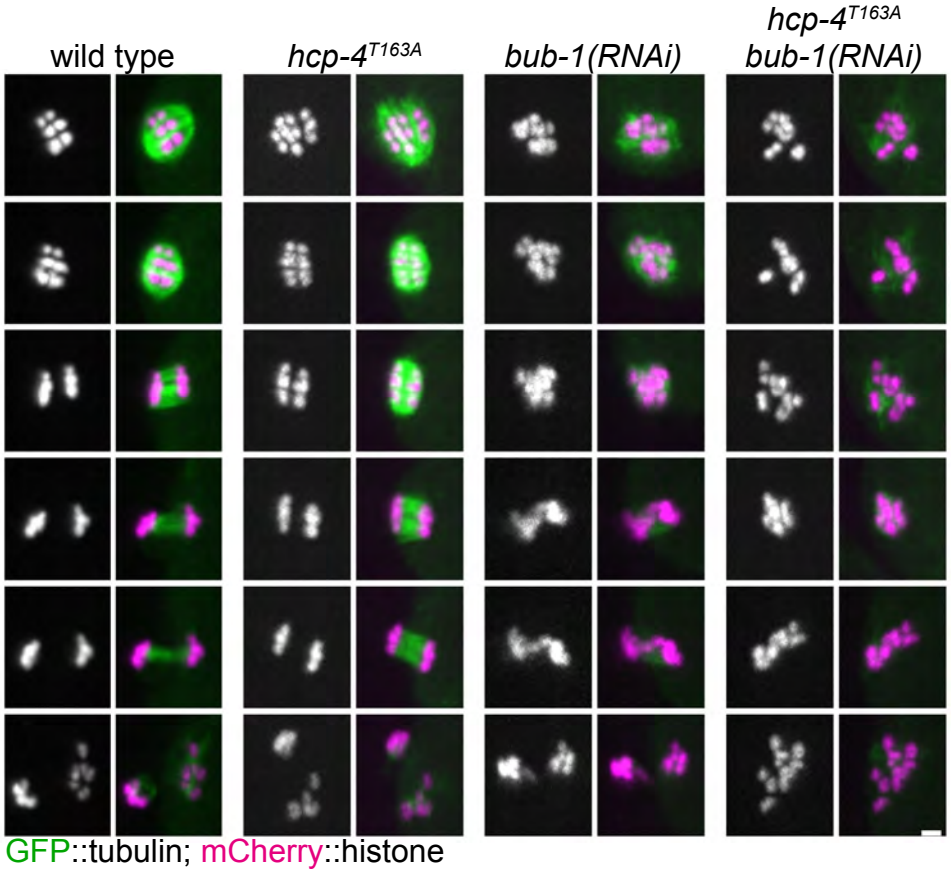
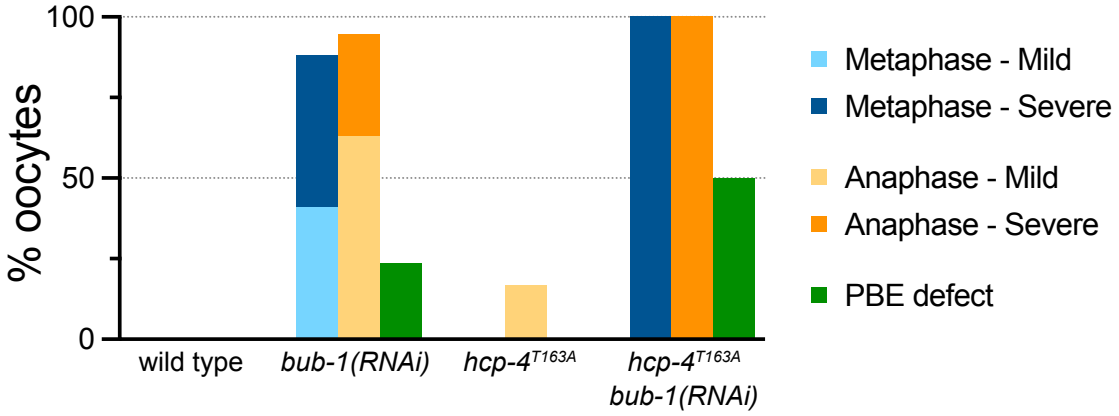
C